Regulation of Interferon-Inducible 2'-5'-Oligoadenylate Synthetases by Adenovirus VA_I RNA

By

Hui Meng

A thesis submitted to the Faculty of Graduate Studies of

The University of Manitoba

in partial fulfilment of the requirements for the degree of

MASTER OF SCIENCE

Department of Chemistry

University of Manitoba

Winnipeg, Manitoba

Abstract

Viral double-stranded RNA is a key pathogen invasion signal recognized by the human innate immune system. All adenoviruses synthesize at least one highly structured RNA (VA_I) to suppress this antiviral response by attenuating the activity of antiviral proteins. Surprisingly, VA_I RNA was previously shown to positively regulate the activity of one interferon-inducible antiviral protein, 2'-5'-oligoadenylate synthetases (OAS). The present thesis focuses on investigating the regulation of a human OAS1 isoform by VA_I RNA and its derivatives. An *Escherichia coli* protein expression and purification system has been developed for OAS1 protein production. A combination of biochemical and biophysical approaches was employed to examine VA_I RNA binding affinity, activation potential for OAS1 and OAS1:VA_I RNA complex formation. Taken together, I have found that while full-length VA_I does indeed activate OAS1 *in vitro*, a truncated version lacking the terminal stem has the opposite effect, and this is the physiologically important response.

Acknowledgments

It is a great pleasure to thank everyone who helped me during my research project and thesis writing. First, I would like to express my gratitude to my supervisor, Dr. Sean McKenna, for his knowledge, his encouragement, his understanding, and his great efforts to explain things simply and clearly. Without his professional guidance and valuable support, this thesis would not have been possible.

I would like to thank other members of my committee, Dr. Joe O'Neil, Dr. Mazdak Khajehpour, and Dr. Teresa De Kievit for their guidance and assistance during thesis writing. I also thank Dr. Mazdak Khajehpour for his insights into developing a quantitative enzyme assay for OAS1 activation and assistance with analysis.

I would also offer my thanks to all the former and current members in Dr. Sean McKenna's Lab. Special thanks go to Soumya Deo for his technical assistance with OAS1 purification and activity assay. Advice given by Dr. Evan Booy and Edis Dzanaovic during my graduate program has been great help and greatly appreciated.

I must thank Dr. Jörg Stetefeld and Dr. John Sorensen research groups for providing access to their equipment and their technical assistance. I must acknowledge Dr. Lynda Donald for her expertise, suggestion and efforts in completion of mass spectrometry analysis. Appreciation also goes to Drs. Ken Standing and Werner Ens for providing access to mass spectrometry instruments, along with Victor Spicer and Dr. Vladimir Collado for their technical assistance.

I also express my gratitude to Natural Sciences and Engineering Research Council of Canada (NSERC) for financially supporting this work.

Finally, I would like to thank my family for all their love and endless support throughout years.

Dedication

I dedicate this thesis

to my husband, Feng Gao, for his support throughout years.

to my boys, Andy and Aiden, for bringing joy and happiness to my life.

to my parents for their love.

Contents

List of Tables

List of Figures

List of Copyrighted Material

Licensed content publisher: Elsevier

Licensed content publication: Journal of Molecular Biology

Licensed content title: Regulation of the interferon inducible 2'-5'-oligoadenylate synthetases by adenovirus VA_IRNA.

Sections where the licensed materials can be found: 2.2.2.1, 2.2.2.2, 2.2.2.3, 2.2.2.4, 2.2.2.5, 2.3.2, 2.4.2, 2.5, 2.6, 2.7, 2.8, 3.1, 3.2, 3.3, 3.4, 3.5, 3.6, 4.1, and 4.2.

List of Abbreviations and Symbols

2’-5’-A	2’-5’-oligoadenylate
5’-OH	5’-hydroxyl
5’-P	5’-monophosphate
5’-PPP	5’-triphosphates
ARD	ankyrin repeat domain
AS	apical stem
ATP	adenosine triphosphate
BME	β-mercaptoethanol
C-F-K	cysteine-phenyalanine-lysine
CARD	caspase recruitment domain
CLA	chloramphenicol
CS	central stem
CV	column volume
DLS	dynamic light scattering
dsRBD	double-stranded RNA binding domain
dsRNA	double-stranded RNA
DTT	dithiothreitol
E. coli	*Escherichia coli*
$EBER_I$	Epstein–Barr virus (EBV)-encoded small RNA I
EBV	Epstein–Barr virus
EDTA	ethylenediaminetetraacetic acid
eIF2α	alpha subunit of eukaryotic initiation factors 2

EMSA	electrophoresis mobility shift assay
Exp 5	exportin 5
f	fraction of bound RNA
FPLC	fast-performance liquid chromatography
HEK293T	human embryonic kidney 293T cell
HIV-I	human immunodeficiency virus type I
HPLC	high performance liquid chromatography
HTLV-1	human T-cell leukemia virus type 1
IFN	interferon
IFNAR1/2	interferon-α/β receptor
IPTG	isopropyl-β-D-thio-galactopyranoside
IRF3	interferon regulatory factor 3
IRF9	interferon response factor 9
ISG	interferon-stimulated gene
ISGF3	interferon-stimulated gene factor 3
ISRE	interferon-stimulated response element
JAK	Janus kinase
KAN	kanamycin
K_{app}	apparent dissociation constant
k_{cat}	turnover number
K_d	dissociation constant
LB	Luria–Bertani
LGP2	laboratory of genetics and physiology2
MALDI	matrix-assisted laser desorption/ionization
MDA5	melanoma differentiation-associated gene 5

MS	mass spectrometry
NADPH	reduced nicotinamide adenine dinucleotide phosphate
NF-κB	nuclear factor kappa-light-chain-enhancer of activated B cells
Ni–NTA	nickle-nitrilotriacetic acid
NMR	nuclear magnetic resonance
NTP	nucleotide triphosphate
OAS	2', 5'-oligoadenylate synthetase
PK	protein kinase-like domain
PKR	protein kinase RNA-dependent
poly I:C	polyinosinic-polycytidylic acid
PPi	pyrophosphate
PRR	pattern-recognition receptors
P_t	protein concentration at equilibrium
PTGS	post-transcriptional gene silencing
R_H	hydrodynamic radii
RIG-I	retinoic acid-inducible gene-I
RISC	RNA-induced silencing complex
RLR	retinoic acid-inducible gene-I-like-receptor
RNAi	RNA interference
RNASE	ribonuclease domain
RNaseL	endoribonuclease L
RxRE	Rex-response element
SDS-PAGE	sodium dodecyl sulfate polyacrylamide gel electrophoresis
SEC	size exclusion chromatography
siRNA	small-interference RNA

STAT	signal transducers and activators of transcription
TAR	trans-activating response region
TEV	tobacco etch virus
TIR	toll/interleukin-1 receptor
TLC	thin-layer chromatography
TLR3	toll-like-receptor 3
TRIF	TIR-domain-containing adapter-inducing interferon-β
TS	terminal stem
V	reaction velocity
VA_I	Adenoviral virus-associated RNA I
V_{max}	maximum reaction velocity

Chapter 1

Introduction

1.1 Literature review

The human innate immune system is the first line of defense against viral invasion. In this system, interplay between viral components [including, viral double-stranded RNA (dsRNA)], type I interferons (IFN), and IFN-inducible antiviral proteins are crucial for antiviral responses. Recognition of viral dsRNA by cellular receptors triggers IFN production and IFN-related antiviral responses in virus-infected cells (1-3). In turn, viral dsRNA regulates the functions of IFN-inducible antiviral proteins (4, 5).

1.1.1 Interferon responses to viral dsRNA

dsRNA produced during the viral life cycle or directly from the viral genome function diversely and interact with key components in the human innate immune system (6-8) (**Fig.1**). Viral dsRNA are recognized by pattern-recognition receptors (PRR) to trigger a signalling cascade and ultimately to induce the expression of IFN in host cells (9-12). Type I IFNs stimulate host cells through a series of signal transduction pathways to express the interferon-stimulated genes (ISG) (8). The protein products encoded by these ISGs are responsible for a series of cellular antiviral responses to inhibit viral replication or enhance immune responses (1). Meanwhile, viral dsRNA also regulate the functions of these antiviral proteins (5).

Figure 1 Interferon responses to viral dsRNA

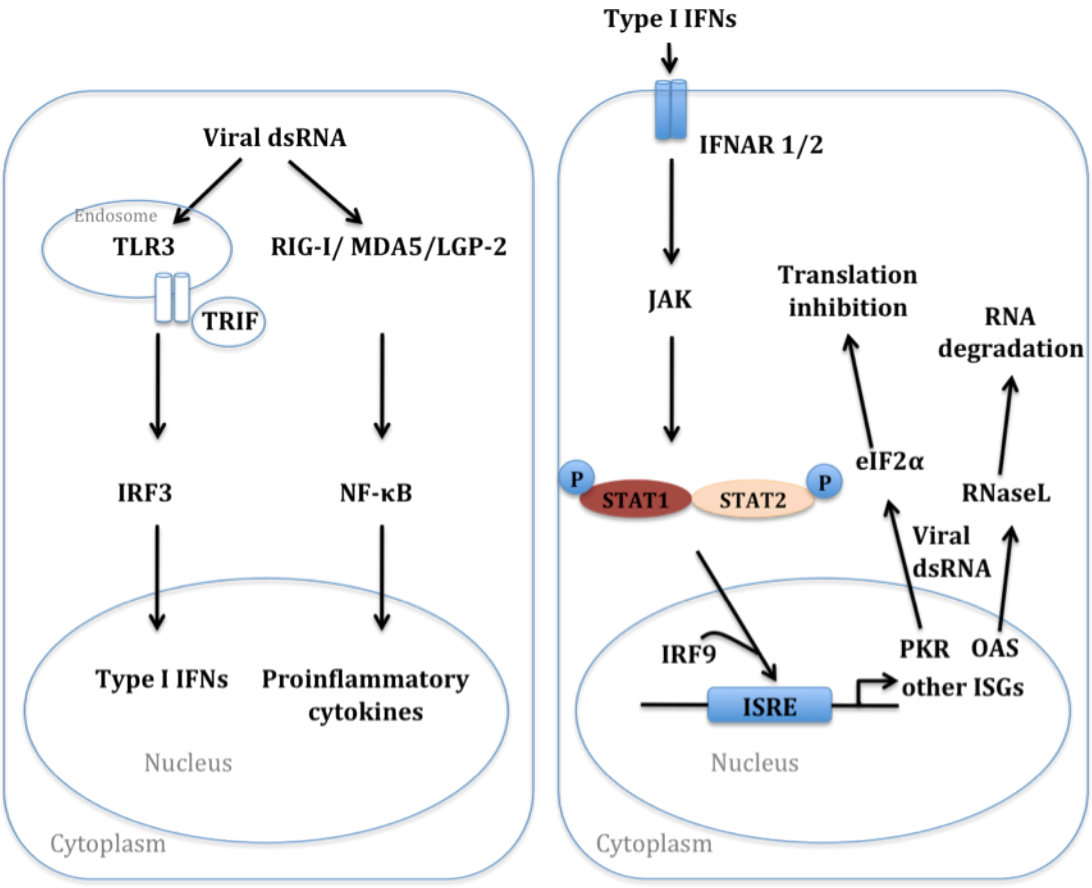

Viral dsRNA is recognized by pattern-recognition receptors in host cells to trigger IFN induction signals (9, 12). The induced IFNs in turn simulate the expression of ISGs to enhance the innate immune antiviral activities to viral infection (8).

1.1.1.1 Viral dsRNA sensing and IFN induction

Viral dsRNA are recognized by PRRs and trigger a signalling cascade to induce the expression of IFNs and proinflammatory cytokines in the host cells. One well-characterized example of a PRR is the toll-like-receptor 3 (TLR3) (10). TLR3 recognizes viral dsRNA and is localized to either the cell membrane or the endosomal membrane (13). Once bound by dsRNA, TLR3 undergoes dimerization and recruits the toll/interleukin-1 receptor (TIR)-domain-containing adapter-inducing interferon-β (TRIF) protein via the TIR domain interaction in both TLR3 and TRIF. This interaction leads to the activation of interferon regulatory factor 3 (IRF3) resulting in the production of type I IFNs, IFN-α/β (14). Activated TLR3 can also activate the nuclear factor kappa-light-chain-enhancer of activated B cells (NF-κB), a crucial transcription factor to regulate the gene expression in both innate and adaptive immune systems (11, 15, 16). Another example of a foreign dsRNA receptor is the retinoic acid-inducible gene-I-like-receptors (RLRs) (12). In this family, three members sharing the common features of dsRNA binding and helicase activity have been identified, and include retinoic acid-inducible gene-I (RIG-I), melanoma differentiation-associated gene 5 (MDA5), and laboratory of genetics and physiology 2 (LGP2) (17, 18). Similar to TLR3, RIG-I and MDA5 also activate signalling pathways to induce the expression of IRF3/7 and NF-κB, and ultimately leads to the induction of IFN-α/β and other cytokines (12). Both RIG-I and MDA5 contain two caspase recruitment domains (CARD), which are employed to interact with CARD-containing adaptor to trigger the downstream signalling (17). Unlike RIG-I and MDA5, LGP2 lacks N-terminal CARDs but has an ATPase domain that facilitates the dsRNA recognition by the first two enzymes (18). Together, viral dsRNA

are sensed by PPRs and trigger a signalling cascade to induce the production of IFN and other cytokines that in turn enhance the host immune responses to viral infections.

1.1.1.2 Inducible expression of ISGs

Upon induction by viral dsRNA signals, the induced type I IFNs are secreted into the intercellular space and bind to the cell-surface interferon-α/β receptors (IFNAR1/2) of surrounding cells resulting in the global expression of ISGs (19). The binding of IFNs to IFNAR1/2 trigger the activation of the Janus kinases (JAK) that in turn phosphorylate and activate the signal transducers and activators of transcription (STAT) (20, 21). STAT1, STAT2 and interferon response factor 9 (IRF9) assemble into a complex with interferon-stimulated gene factor 3 (ISGF3), which binds to the interferon-stimulated response element (ISRE) localized in the promoter sequences of ISGs (22, 23) (**Fig.1**). The expressed protein products of these ISGs, also known as IFN-inducible antiviral proteins, are involved in many IFN-associated antiviral, antiproliferative and immunoregulatory responses (8, 24). Two key examples are IFN-inducible and dsRNA-binding proteins, 2'-5'-oligoadenylate synthetases (OAS) and protein kinase RNA-dependent (PKR) (25). As proven IFN-inducible antiviral proteins, both OAS and PKR suppress the protein translation required for virus assembly and replication, and are also involved in the downstream signalling transduction to amplify the cellular immune responses to viral infections (26, 27). OAS enzymes, upon interaction with dsRNA, become activated and polymerize ATP into 2'-5'-oligoadenylate (2'-5'-A) chains (28, 29). These oligoadenylate chains bind to and activate endoribonuclease L (RNaseL), which destroys RNA from the ribosome and virus itself, thereby restricting viral propagation (30, 31). The small RNA resulting from RNaseL cleavage can in turn act on

two pathogen recognition receptors, RIG-I and MDA5, to initiate IFN induction and amplify the antiviral responses (32, 33). Upon dsRNA binding, latent PKR undergoes dimerization and autophosphorylation to become active (34). The activated dimeric PKR phosphorylates the alpha subunit of eukaryotic initiation factors 2 (eIF2α) on its Ser51 site to inhibit protein translation in the virus-infected cells (34-36). In addition to eIF2α phosphorylation, PKR also interacts with other cellular proteins which function in RNA metabolism, such as RNA helicase A and human immunodeficiency virus type 1 (HIV-1) Tat (37, 38). Another key role of PKR is to regulate translation factors independent of phosphorylation. It has been demonstrated that PKR without kinase activity is capable of activating NF-κB (39).

1.1.1.3 Regulation of IFN-inducible antiviral proteins by viral dsRNA

Viral dsRNA also regulates the enzymatic functions of IFN-inducible antiviral proteins (5). In order to circumvent the IFN responses to viral infections, one strategy that viruses use is to generate highly-structured small RNA molecules to inhibit the activity of IFN-inducible antiviral proteins (3). The best-characterized example is the negative regulation of PKR by specifically transcribed viral dsRNA. Both Epstein–Barr virus (EBV)-encoded small RNA I ($EBER_I$) and adenoviral virus-associated RNA I (VA_I) have been shown to bind to PKR with similar affinity as dsRNA activators but prevent the self-association and autophosphorylation of the enzyme (40). In this way, the protein synthesis crucial for virus assembly can proceed unimpeded. In the case of OAS enzymes, however, it has been demonstrated that most characterized viral dsRNA serve as OAS activators, including $EBER_I$ (41), VA_I (42), Rex-response element (RxRE) of human T-cell leukemia virus type 1 (HTLV-1) (43), and trans-activating response region

(TAR) of HIV-1 (44). The basis for the opposite roles played by viral dsRNA (e.g. $EBER_I$ and VA_I) with OAS and PKR remains poorly understood, which was the main source for my research project. In addition to regulating OAS, it has been shown that viral RNA can inhibit the OAS downstream effector RNaseL (45). An RNA structure from a poliovirus open reading frame inhibits the RNA cleavage ability of RNaseL during the early stages of infection (46).

Taken together, viral RNAs generated during virus replication cycles play diverse roles in the host IFN antiviral system. These RNAs serve as viral stress signals to trigger the induction of type I IFNs, as regulatory cofactors for IFN-inducible antiviral proteins and also as the acting targets of host antiviral activities. These functions all involve the interactions between host proteins and viral RNAs. Thus examination of such interactions would clarify our understanding of how the host defence system detects the viral invasion and aid finding potential RNA therapeutic agents for either viral or autoimmune diseases. In my thesis, I sought to understand the regulation of OAS activity by adenoviral VA_I RNA. In the following sections, key details about OAS-RNaseL system and VA_I RNA will be reviewed to place my results in the proper context.

1.1.2 OAS-RNaseL system

The OAS-RNaseL system is a key player in degradation of viral and cellular RNA in virus-infected cells. OAS enzymes were discovered more than 35 years ago, resulting from the demonstration that protein synthesis is blocked by dsRNA from IFN-stimulated cells (47, 48). These enzymes are unique in that they catalyze the formation of 2'-5'-phosphodiester bonds instead of 3'-5'-phosphodiester ones (**Fig.2**). Upon induction

by IFN and binding to dsRNA, OAS enzymes polymerize adenosine triphosphate (ATP) into 2'-5'-oligoadenylates (2'-5'-A), which are the only known activators for the antiviral endoribonuclease, RNaseL (**Fig.3**). In turn, the activated RNaseL degrades both viral and cellular RNA to inhibit protein synthesis and block viral infection (30, 49). The key mechanistic steps involved in this pathway are: (i) RNA binding and activation of OAS, (ii) catalytic formation of 2'-5'-A , (iii) activation of latent RNaseL, and (iv) degradation of RNA by RNaseL. The details of each step will be discussed below.

Figure 2 OAS enzyme reaction

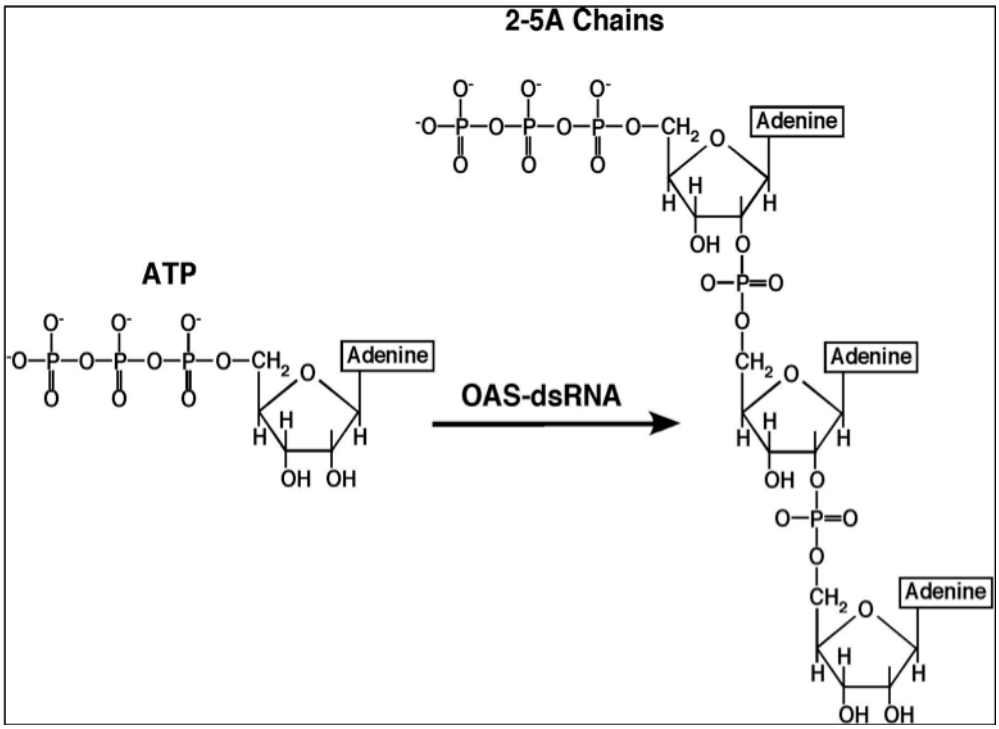

OAS enzymes catalyze the unique 2'-5'-A chain formation instead of 3'-5'-A chains (67).

Figure 3 OAS/RNaseL pathway

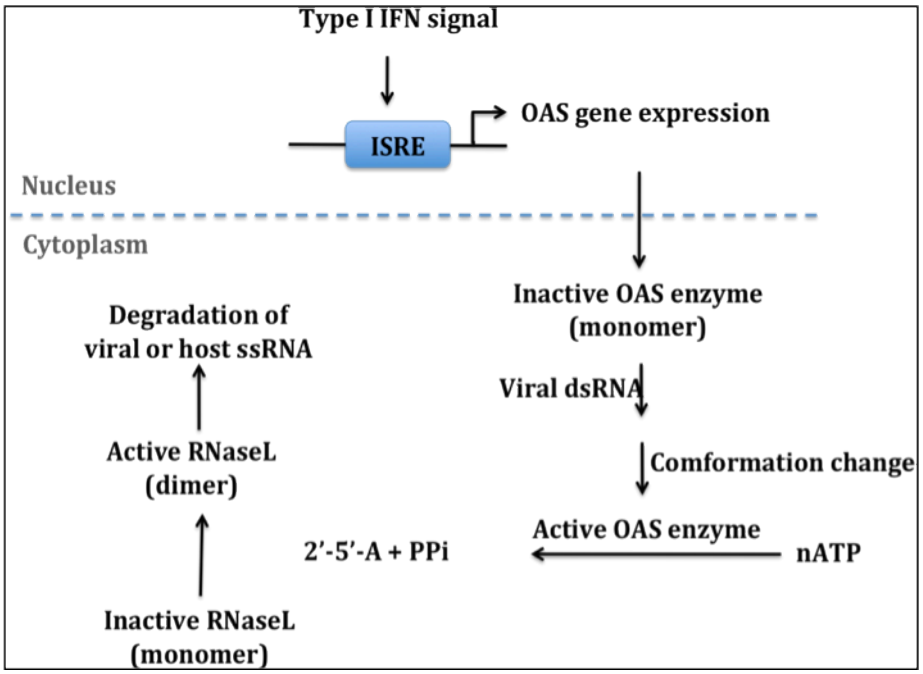

OAS gene expression is induced by the IFN cascade. OAS enzyme is activated in the presence of dsRNA and catalyzes the formation of 2'-5'-A, which in turn activates latent RNaseL to initiate the degradation of viral or host RNA in virus-infected cells (49, 30).

1.1.2.1 RNA binding and OAS activation

Generally, human OAS enzymes are classified into three functional forms based on the numbers of the core OAS units. OAS1, OAS2 and OAS3 contain one, two and three OAS units, respectively (50, 51) (**Fig.4**). In OAS1, the core OAS unit includes the first 346 N-terminal amino acids (52). In addition to these three forms, OASL (OAS like protein) has one OAS unit and two ubquitin-like domains but is devoid of the OAS enzymatic activity (53, 54).

Figure 4 Domain organization in OAS enzymes

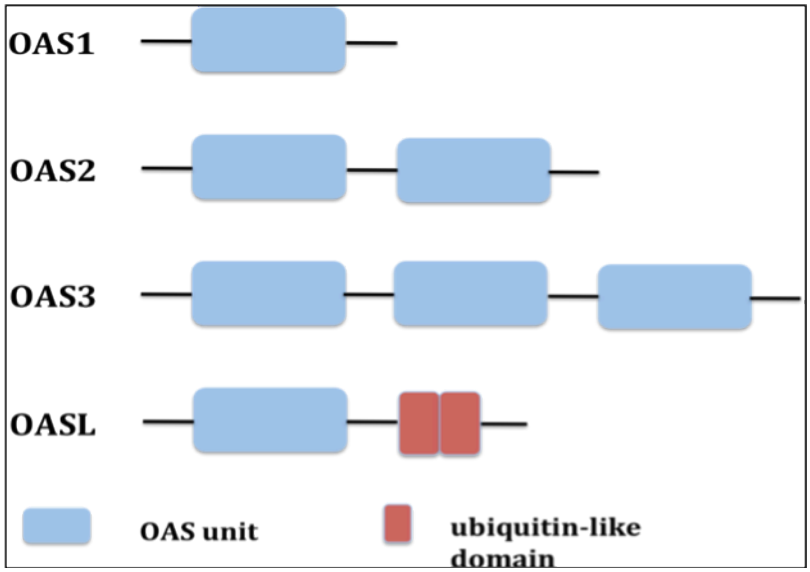

OAS1, OAS2 and OAS3 contain one, two and three OAS units, respectively (50, 51). OASL (OAS like protein) has one N-terminal OAS unit and two C-terminal ubquitin-like domains (54).

OAS enzymes are expressed at low constitutive levels in human cells. Once induced by type I IFNs, inactive OAS accumulates in the cytoplasm. Upon binding to and activation by viral dsRNA, inactive OAS1 and OAS2 enzymes are proposed to convert into the active forms via oligomerization (55). It has been found that the mutation of C-F-K (cysteine-phenyalanine-lysine) amino acid residues located in the core OAS unit of OAS1 and OAS2 significantly affected the tetramerization and dimerization of OAS1 and OAS2, respectively (56). There is no C-F-K motif in either OAS3 or OASL, and therefore their active forms are proposed to remain monomeric (56). However, monomeric and fully active OAS1 has been observed by two groups (57, 58).

Thus, the importance of self-association of OAS enzymes for enzymatic activation needs further investigation.

OAS enzymes are a highly conserved family but share no considerable sequence homology to other known dsRNA-binding proteins or to any known dsRNA-binding motif. According to the high-resolution crystal structure of porcine OAS1, a positively charged groove on the back face of the bilobal structure, roughly parallel to the active site, is the putative dsRNA-binding site (59). Hartmann and colleagues observed that the binding affinities of different aptamers to OAS1 do not couple with their activation abilities, which supports a two-step process for OAS activation (60). First, dsRNA binds to the OAS enzyme in a relatively non-specific way followed by a conformation change to OAS enzyme structure. The structural rearrangement of OAS enzyme is hypothesized to enable the easy access of substrate to the active site. The activation of OAS enzymes depends on a number of dsRNA properties including the length (e.g.>15 bp ds region), sequence composition, nucleotide modification, secondary structure and deviations from perfect RNA duplex (60-64). Polyinosinic-polycytidylic acid (poly I:C) is a synthetic analog of dsRNA (average molecular weight ~ 200 KDa) and conventionally used as an activator for OAS enzymes. As a immunostimulant, polyI:C is a good tool for immunology research as it will induce the IFN cascade. However, in order to understand the interaction between OAS enzymes and their natural dsRNA activators, polyI:C is inappropriate and actual viral dsRNA need to be examined.

1.1.2.2 Catalytic formation of 2'-5'-A

The enzymatic activity to form 2'-5'-linked oligonucleotides instead of 3'-5'-linked oligonucleotides is a unique feature of OAS enzymes. The active site of OAS enzymes is localized at the interface between N- and C- terminal domains in the core OAS unit (59). The N-terminal domain of each OAS unit contains the three aspartic residues that are thought to coordinate two Mg^{2+} ions required for catalysis, typical of the nucleotidyl transferase family. The helical turn sequence containing a Gly-Ser motif also exists in the N-terminal domain of the OAS unit that is thought to interact with the donor ATP via a hydrogen bond with serine (29, 59, 65). However, the mechanism of interaction with the acceptor ATP and how the 2'-hydroxyl reacts with the donor α-phosphate moiety remains unclear. According to structural and mutagenesis analysis, it is believed that the 2' specificity of the OAS enzyme depends on the orientation of the acceptor ATP to enable the 2'-hydroxyl to react (59, 65).

The types of 2'-5'-A chain synthesis vary among OAS enzymes. OAS1 and OAS2 are able to synthesize trimer and tetramer 2'-5'-A species and even longer under the optimized condition *in vitro*, whereas OAS3 primarily catalyzes the formation of dimeric 2'-5'-A which is not an efficient activator of RNaseL (66, 67). It is therefore hypothesized that OAS3 may function in other cellular processes unrelated to RNaseL-mediated RNA degradation.

1.1.2.3 Activation of RNaseL and degradation of RNA by RNaseL

The only established biological function of 2'-5'-A is to activate RNaseL. The latent RNaseL is widely expressed in most human tissues as an inactive monomer (68).

The main domains of RNaseL are ankyrin repeat domain (ARD), protein kinase-like domain (PK) and ribonuclease domain (RNASE) (69). 2'-5'-A with qualified length (at least trimer) binds to the ARD domain, which triggers the homodimerization of latent RNaseL monomer (49). The active RNaseL cleaves ssRNA via its RNASE domain (69, 70). Active RNaseL degrades the viral genomic RNA and acts on the viral mRNA to block viral protein synthesis. The RNaseL substrates come not only from the viral genome themselves, but also from the host cell (68). RNaseL also degrades host cellular RNAs including mRNA and rRNA in such a way to destroy the host cell machinery that is required for virus replication and eventually decrease the viability of virus. In turn, small RNA products from RNaseL cleavage can induce IFN-β to amplify the IFN immune responses (49). Evidence has also shown that RNaseL may induce apoptosis in virus-infected cells to prevent virus from spreading to the healthy cells (71).

1.1.3 Adenoviral virus-associated RNA I, VA_I RNA

The focus of my thesis is to investigate the interaction between a specific viral RNA, VA_I from adenovirus and OAS1 enzyme. Adenoviruses are nonenveloped viruses that are composed of a linear double-stranded DNA genome and a capsid. These viruses are mainly responsible for upper respiratory infections, especially in children. Outcomes associated with adenovirus infection vary from common cold to pneumonia, croup and bronchitis (72). The genomes of most adenovirus serotypes encodes two non-coding small virus-associated RNAs, VA_I and VA_{II} and are produced in the infected host cells by using host transcription machinery (73). VA_I RNA is the major species, which reaches ~10^8 copies (μM concentration) during late stages of viral replication, whereas

VA_{II} RNA is the minor species (maximum ~10^6 copies) (73, 74). They each contain approximately 160 nucleotides and fold into secondary structures containing primarily dsRNA stem-loops (**Fig.5**) (74). Since VA_I RNA is the major species, most studies have been focused on this molecule. VA_I RNA is transcribed in the nucleus by host RNA polymerase III, and then transported by exportin 5 (Exp 5) to the cytoplasm in the adenovirus-infected cell (75). The secondary structure of VA_I RNA features three major domains: the terminal stem (TS), the central stem (CS), and the apical stem (AS) (**Fig.5**). TS and AS domains are imperfectly base-paired, and CS is a structurally complex domain (76).

Figure 5 VA_I RNA secondary structure

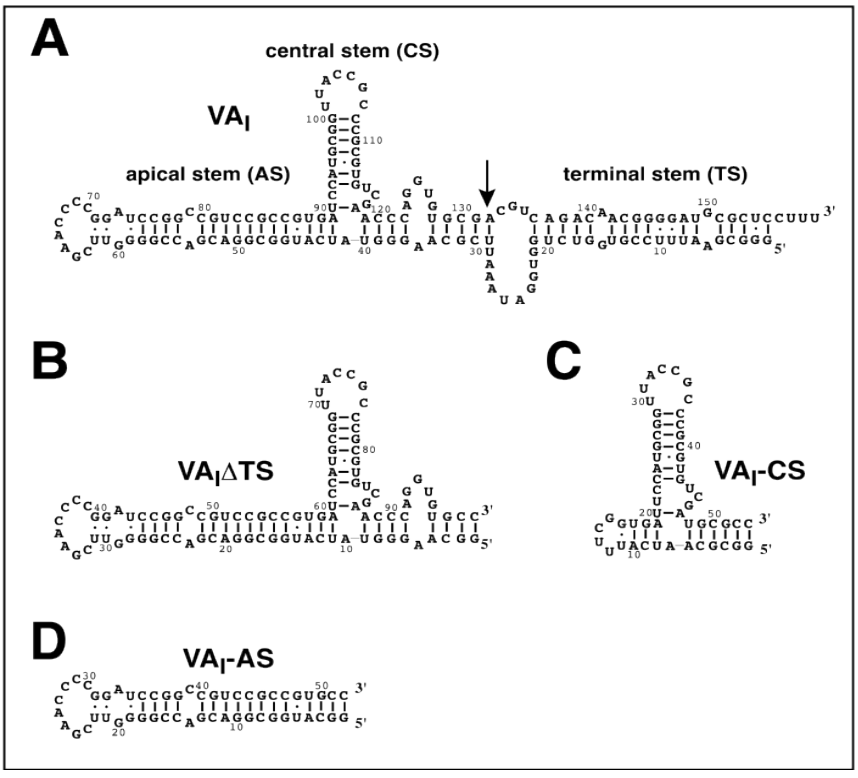

Secondary structures of **(A)** adenovirus VA_I RNA (40) with the Dicer cleavage site indicated by an arrow, **(B)** the terminal stem truncation ($VA_I\Delta TS$) (85), **(C)** the central stem loop alone (VA_I-CS), and **(D)** the apical stem-loop alone (VA_I-AS).

VA_I RNA is required for viral mRNA translation during late stages of infection, and plays key role during viral replication by directly interacting with innate immunity protein partners in virus-infected cells (73, 75). Studies have shown that VA_I RNA induces IFN production via the RIG-I signalling pathway, blocks the activation of PKR to allow the viral and host protein synthesis to proceed, serves as the substrate for Dicer to generate small RNAs acting as a small-interference RNA (siRNA) and acts on OAS1 enzyme as an RNA activator (40, 42, 77, 78). Details on each of these key interactions with innate immune proteins are discussed below.

1.1.3.1 VA_I RNA and PKR

VA_I RNA acts as a competitive inhibitor to block the activation of PKR, thus preventing dsRNA activators from binding to this antiviral protein (79, 80). Binding of VA_I RNA to PKR is achieved via the AS domain binding to the double-stranded RNA binding domains (dsRBD) of PKR, whereas inhibition also requires the central domain of VA_I RNA (81). VA_I RNA has a similar affinity for PKR as other viral dsRNA activators, and this binding prevents the required self-association of PKR for activation (40). Without self-association, PKR autophosphorylation is attenuated and the kinase activity is also inhibited so that protein synthesis proceeds at normal level in virus-infected cells (40).

1.1.3.2 VA_I RNA and OAS

A single study has demonstrated that full-length VA_I RNA activates the murine OAS enzyme, which is paradoxical given the inhibitory role that VA_I RNA plays with respect to PKR (42, 80). The main observation of this study is that VA_I RNA binds to

and activates the murine OAS enzyme that was expressed recombinantly in bacterial cells. They also showed that the long duplex regions in the AS and TS domains were crucial for OAS activation. When the imperfectly base-paired regions were converted into perfect base pairs, the OAS activation potential was dramatically increased. Meanwhile, disruption of the CS domain led to a reduction in OAS activation but did not affect binding. However, the authors did not define the specific VA_I RNA domains responsible for OAS binding and activation.

1.1.3.3 VA_I RNA and Dicer

RNA interference (RNAi) is a naturally occurring post-transcriptional gene silencing (PTGS) process mediated by dsRNA eventually leading to the degradation of target homologous mRNA (82). Dicer is a key dsRNA-specific endoribonuclease at the heart of the RNAi pathway (83). Longer initiating dsRNA is processed by Dicer into siRNA approximately 22 nucleotides long, which is unwound and incorporated into an RNA-induced silencing complex (RISC) to target mRNA matching the source RNA for degradation (6, 83). Recent studies have shown that VA_I RNA serves as a substrate for Dicer (78, 84). Both *in vitro* and *in vivo* studies have shown that VA_I RNA is processed by Dicer between CS and TS domains to form one long and one short dsRNA (**Fig.5**) (84, 85). The long dsRNA binds to and inactivates PKR to enable continued protein synthesis in virus-infected cells (85). One of the strands from the processed short dsRNA (equivalent to the TS domain) is incorporated into an active RNA-induced silencing complex (78, 84, 86). Therefore, the current data points to the enticing possibility that a single VA_I molecule may simultaneously antagonize both the RNA interference machinery (via a processed terminal stem) and the interferon response (via the remaining

apical and central stems). It also suggests that VA_I RNA may exist as three different forms *in vivo*, full-length VA_I, AS-CS domain and TS domain alone.

1.1.4. Viral RNA sensing through 5'- end modifications

A final feature to be introduced is the concept of how a host cell differentiates self- from foreign dsRNA. The presence of a 5'-triphosphate group is a signature of viral RNA that is distinct from the mature host RNA present in the cytoplasm (87-89). Initially, host mRNAs are transcribed with a 5'-triphosphate group in the nucleus, but are rapidly processed through post-transcriptional modifications, including cleavage, 7-methylguanosine capping, polyadenosine tail addition and base modification, and then transported into the cytoplasm as a mature mRNA (90). Viral dsRNA sensors (for instance, PKR and RIG-I) that exist in the cytoplasm can distinguish viral from self RNA through the recognition of 5'-triphosphate group on viral RNAs. It has been reported that PKR can be activated by short stem-loop RNA in a 5'-triphosphate-dependent fashion (91). RIG-I, as an innate immune sensing helicase, has also been demonstrated to recognize RNA stem-loops through a 5'-triphosphate group (87). The role of 5'-triphosphate group on viral RNA has not been investigated for OAS enzymes.

1.2 Thesis overview

2'-5'-OAS and PKR are interferon-inducible, dsRNA binding, antiviral enzymes (25). The mechanism of interactions between PKR and its dsRNA-binding partners has been reasonably well characterized, as several viral dsRNAs have been investigated (38, 40, 43, 44, 92, 93). Due to the difficulty in OAS enzyme purification and the low affinity

binding with its dsRNA cofactors, the molecular basis of OAS-dsRNA interactions remains unclear. One study has shown that human adenoviral virus-associated type I RNA, VA_I RNA binds to and activates OAS enzyme *in vitro* (42), whereas studies have demonstrated that VA_I RNA binds to and inactivates PKR (40, 85). The paradoxical roles played by VA_I RNA with respect to OAS and PKR regulation forms the basis for this thesis. The secondary structure of VA_I RNA features three major domains: the terminal stem (TS), the central stem (CS), and the apical stem (AS) (75). Recent investigation suggested that VA_I RNA is processed by Dicer into two species: a TS-lacking VA_I RNA and small RNA from TS *in vivo* (84). In light of this discovery that Dicer efficiently truncates VA_I, we decided to investigate the regulation of the specific OAS1 isoform (p42) by both the full length VA_I and a series of truncated molecules, including one that corresponds to the Dicer-processed version lacking the terminal stem ($VA_I\Delta TS$). No studies to date have shown the effects of $VA_I\Delta TS$ on OAS enzymes. The role of individual VA_I RNA stem-loops (e.g. AS and CS) during interaction with OAS also remains unclear. Thus, one goal of my research project is to characterize the particular regions of VA_I RNA that contribute to the activation of OAS and determine the regulatory effect of VA_I RNA on OAS activity by biochemical and biophysical approaches. The other goal of my project is to identify the structural characteristics of OAS-VA_I RNA complex by structural biology methods.

In order to achieve the goals mentioned above, an *Escherichia coli* (*E. coli*) protein expression and purification system has been developed and optimized for recombinant human OAS1 p42 isoform production. Full-length VA_I RNA and its truncated forms, including VA_I-AS, VA_I-CS, VA_I ΔTS (a mimic of Dicer-processed VA_I

RNA) RNAs were transcribed by T7 polymerase and isolated through an extensive purification procedure. A rapid and simple colorimetric method was developed to determine OAS activation by VA_I RNA and its truncated forms by detecting pyrophosphate (PPi) released by 2'-5'-A formation from ATP. Activation assays demonstrated the ability of different RNAs to stimulate 2'-5'-A chain formations; full-length VA_I RNA activates OAS1 whereas VA_I ΔTS does not. Electrophoretic mobility shift assays (EMSA) were employed to determine the binding affinity of each RNA for OAS1. Only VA_I ΔTS was capable of forming detectable complexes with OAS enzyme. EMSA results also suggested that VA_I ΔTS forms two higher molecular weight complexes with OAS. Further, a novel non-denaturing mass spectrometry (MS) approach was used to characterize VA_IΔTS-OAS complexes. VA_IΔTS-OAS complexes were identified at 1:1 and 1:2 ratios by MS under non-denaturing conditions. Additionally, the importance of the RNA 5'-end phosphorylation state to its ability to regulate OAS1 activity has been investigated.

Taken together, using a combination of biochemical approaches, we characterize both the RNA-protein complex formation and activation/inhibition potential of full length VA_I and a series of truncated molecules. Our conclusion is that while full-length VA_I does indeed activate OAS1 *in vitro*, the Dicer-truncated molecule lacking the terminal stem has the opposite effect.

Chapter 2

Materials and Methods

2.1 Introduction

Our main goal was to characterize the ability of VA_I RNA to regulate a key IFN-inducible member of the innate immune response, OAS1. A necessary precursor to these studies was to prepare and purify OAS1 enzyme and VA_I RNA with high yield and purity to perform biochemical and biophysical characterizations. For OAS1 purification, an *E. coli* expression and purification procedure was developed and optimized. Once optimized, OAS1 enzyme could be expressed and purified within one week at a reasonable yield (1.5 to 2.0 mg /L cell culture). Five human OAS1 isoforms (p42, p44, p46, p48 and p52) have been identified that are generated through the alternative splicing of the same gene (52, 94). These OAS1 isoforms have the identical first 346-animo acids and differ in the c-terminal domain. Since OAS1 p42 is the smallest and simplest (18 animo acids in the C-terminus), we decided to start with this specific isoform. For RNA purification, an established plasmid-based *in vitro* transcription procedure was employed to synthesize VA_I RNA and its truncated derivatives. Pure RNA species could be generated in one week at a high yield for biochemical and structural studies. Further, a colorimetric assay was developed for OAS enzymes to eliminate the need for radioactive ATP. To examine VA_I RNA-OAS1 complexes, EMSA, dynamic light scattering (DLS), and MS were used. Finally, the importance of RNA 5'-end phosphorylation state to its

ability to regulate OAS1 activity was investigated by 5'-end dephosphorylation of *in vitro* transcribed RNA. The details of each procedure used will be discussed in the following sections (2.2-2.8).

2.2 OAS1 purification

2.2.1 Overview

It has been over 35 years since OAS enzymes were discovered as IFN-inducible antiviral proteins (47, 48). In the early 1980s, OAS enzymes were mainly purified from IFN-treated cell cultures by employing ammonium sulfate precipitation and polyinosinic-polycytidylic-cellulose (95, 96). With the development of recombinant protein expression systems, OAS enzymes have been expressed in different types of cells, including bacterial and insect cells (97-99). A baculovirus-insect cell system has been employed to express both OAS1 and OAS2 enzymes (98, 100). Compared to the *E. coli* expression system, the baculovirus-insect cell system has two main drawbacks: high-cost cell-culture media and long cell-growth cycles. Unfortunately, it has been shown that the yield of OAS enzymes expressed in *E. coli* cells is low due to inclusion body formation (99, 101). Since *E. coli* expression systems have the advantage of low cost, fast cell-growth rate, simplicity and high expression level, we decided to express a specific human OAS1 (isoform p42) in BL21-CodonPlus(DE3)-RIL *E. coli* cells. The specific BL21-CodonPlus(DE3)-RIL *E. coli* cells contain extra tRNA genes rarely found in *E. coli* cells but used by human cells, which can reduce the codon bias effect on target protein expression (102). In order to increase the solubility of the target protein, the human *oas1tv2* gene was inserted into a non-commercial pET30a(+)-GNSHT vector.

This expression vector codes for a fusion protein containing, from N- terminus to C-terminus, the highly soluble GB1 domain (**G**) from protein G of group G *Streptococcus*, the highly soluble NusA protein (**N**) from *E. coli*, a streptavidin tag (**S**), an 8×His tag (**H**), a TEV protease site (tobacco etch virus, **T**), and *OAS1tv2* (encoding the OAS1 p42 isoform) (**Fig.6**). GB1 domain and NusA proteins increase the solubility of over-expressed protein in solution (103). The 8×His tag is used to separate the GNSHT-OAS1 fusion protein from the total protein in the cell lysate (104). The TEV protease recognition site (E-N-L-Y-F-**Q-S**) is employed to cleave the GNSHT tag off OAS1 to generate the tag-free target protein (105). After TEV cleavage, OAS1 itself still remains soluble in solution. The final yield of OAS1 enzyme is about 1.5-2.0 mg per liter cell culture. Thus, by employing the pET30a(+)-GNSHT vector and BL21-CodonPlus (DE3)-RIL *E. coli* cells, the OAS1 enzyme was expressed and purified at a reasonable yield for our studies.

Figure 6 GNSHT-OAS1 coding region of pET30a(+)-GNSHT-*OAS1tv2*

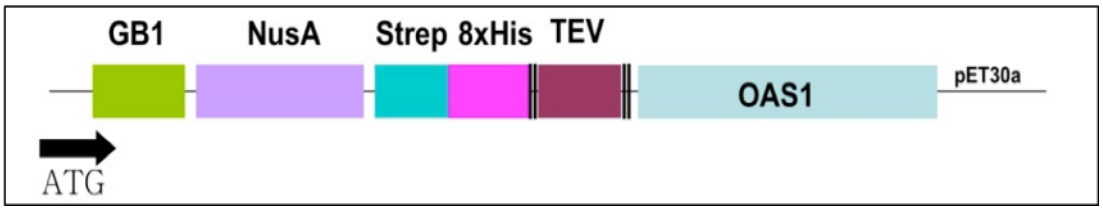

From N- terminus to C- terminus, the highly soluble protein G domain B1 (GB1), the highly soluble NusA protein (NusA), a streptavidin tag (Strep), an 8×His tag (8×His), a TEV protease site (TEV), and *OAS1tv2* (OAS1).

2.2.2 Procedures

2.2.2.1 Construction of pET30a(+)-GNSHT-*OAS1* expression vector

The original *oas1tv2* gene on the plasmid pOTB7 (Open Biosystems) was used as template for PCR amplification using the following primers: 5'OAS1-GNSHT (*GCGCGCGCGTCGACATGATGGATCTCAGAAATACCCCAGCCAAATCTCTGGACA AGTTCATTGAAGACTATCTCTTGCC*) and 3'OAS1-GNSHT (*GCGCGCGCGCGGCCGCTCAAGCTTCATGGAGAGGGGCAGGGATGAATGGCAGG GAGGAAGCAGG*). The resulting PCR product was ligated into a modified pET30a(+) vector (pET30a(+)-GNSHT) (supplied by Dr. Tinghe Wu, Stanford University) in the multiple cloning site to generate the pET30a(+)-GNSHT-*OAS1tv2* expression vector shown as in **Fig.6**. All restriction enzymes and buffers were purchased from NEB (*New England Biolabs*), and the ligation was performed following the Quick Ligation™ Kit protocol from NEB.

2.2.2.2 Expression and IPTG-induction of GNSHT-OAS1 fusion protein

The overexpression of GNSHT-OAS1 enzyme in *E. coli* cells followed a standard protein expression procedure. The pET30a(+)-GNSHT-OAS1tv2 construct was transformed into BL21-CodonPlus(DE3)-RIL competent *E. coli* cells. A single freshly transformed colony from an Luria–Bertani (LB) agar plate containing 20 μg/ml chloramphenicol (CLA) and 30 μg/ml kanamycin (KAN) was inoculated into 10 ml of LB liquid broth containing the same antibiotics. The concentrations of antibiotic stocks are 20 mg/ml (CLA in methanol) and 30 mg/ml (KAN in water). After growing at 37°C for 12-14 h, the 10 ml starter culture was transferred into 1 L LB liquid broth

supplemented with the same antibiotics and grown at 37°C. When the OD_{600} value reached 0.6-0.8, the cell culture was cooled on ice for 15 min, and then the inducing reagent, isopropyl-β-D-thio-galactopyranoside (IPTG), was added to a final concentration of 1 mM. During the cooling period, the incubator was cooled down to 22°C. Then the cell culture was grown at 22°C with shaking at 200 rpm for an additional 16 h to express the protein.

2.2.2.3 Isolation of GNSHT-OAS1 fusion protein from cell lysate by affinity chromatography

The induced bacterial cells were collected by centrifugation at 6,000 × g for 15 min at 4°C, and then the cell pellets were resuspended in cell lysis buffer (50 mM Tris-HCl, 1 M NaCl, 1 mM imidazole, 5% glycerol and 1 mM DTT, pH 7.5). The resuspended cells were disrupted by sonication on ice (20 s pulses at 30 s intervals for 10 cycles) followed by centrifugation at 35,000 × g for 40 min at 4°C. The cell pellets were discarded and the supernatant was transferred into dialysis tubing with a 10 KDa cut-off and dialyzed in wash buffer (50 mM Tris-HCl, 1 M NaCl, 10 mM imidazole, 5% glycerol and 1 mM DTT, pH 7.5) to adjust the pH of lysate to 7.5. The cell lysate was then loaded onto a Ni–NTA (nickel-nitrilotriacetic acid) gravity-flow column [10 ml column volume (CV), QiaGen Inc.] equilibrated with wash buffer. The Ni-NTA column is conventionally used to purify His-tagged protein. The flow-through was collected and reloaded onto the same column. After loading cell lysate, the column was washed with 25×CV of wash buffer to remove the non-specifically bound proteins. Then, immobilized protein was eluted into 10-ml fractions by addition of 10×CV of elution buffer (50 mM Tris-HCl, 300 mM NaCl, 100 mM imidazole, 5% glycerol and 1 mM DTT, pH 7.5). Fractions were checked by

8% SDS-PAGE (sodium dodecyl sulfate polyacrylamide gel electrophoresis) running in 1× SDS-PAGE running buffer. GNSHT-OAS1 protein is mainly found in the first three fractions (**Fig.7**).

Figure 7 Denaturing SDS-PAGE analysis of GNSHT-OAS1 fractions from Ni-NTA column

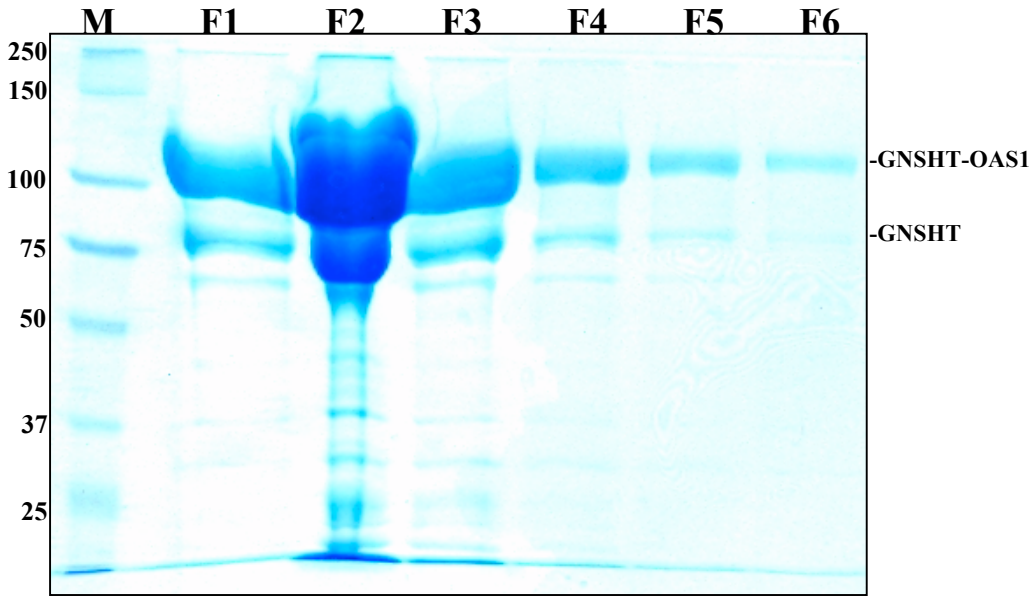

From left to right, lanes correspond to molecular weight markers, eluted fractions 1 to 6 from Ni-NTA column. The 8% SDS-PAGE was run at 150 V and stained with Coommassie blue. **F** indicates the fraction eluted from Ni-NTA column. The migration of fusion protein (GNSHT-OAS1) and the affinity tag (GNSHT) are indicated.

2.2.2.4 Cleavage of GNSHT-OAS1 fusion protein by TEV protease and purification via size exclusion chromatography

The eluate containing the GNSHT-OAS1 fusion protein from the Ni-NTA column was pooled and dialyzed against TEV protease working buffer (50 mM Tris-HCl,

100 mM NaCl, 1 mM EDTA, 5% glycerol and 1 mM DTT, pH 7.5). Then, the GNSHT-OAS1 fusion protein was incubated with TEV protease made in-house at room temperature for 16 h and the reaction was carried out in the dark. The next day, the TEV protease-treated fusion protein was checked by 8% SDS-PAGE to confirm the cleavage efficiency (**Fig.8**).

Figure 8 SDS-PAGE analysis of TEV cleavage of GNSHT-OAS1 fractions

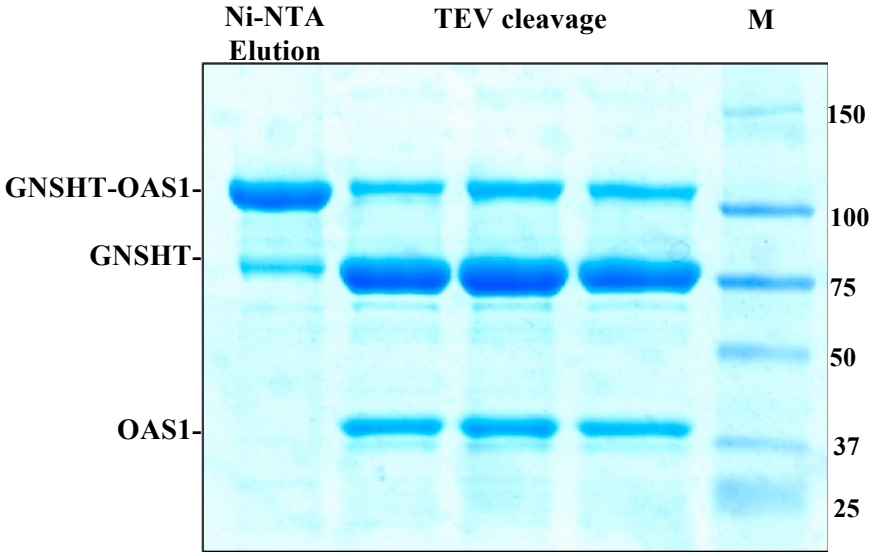

From left to right, lanes correspond to fraction from Ni-NTA column, cleavage of the fusion protein with TEV protease, and molecular weight markers (same as shown in **Fig.7**). The 8% SDS-PAGE was run at 150 V and stained with Coommassie blue. The migration of fusion protein (GNSHT-OAS1), the affinity tag (GNSHT), and OAS1 protein are indicated. TEV cleavage reactions were performed in triplicates under the same conditions.

Next, the cleaved protein was isolated via size exclusion chromatography (SEC) on HiLoad Superdex 200 (26/60, GE Healthcare) performed at 3 ml/min with storage buffer (50 mM Tris-HCl, 100 mM NaCl, and 1 mM DTT, pH 7.5). The SEC elution profile of OAS1 is shown in **Fig.9**.

Figure 9 Size exclusion chromatography (SEC) elution profile of OAS1 purification

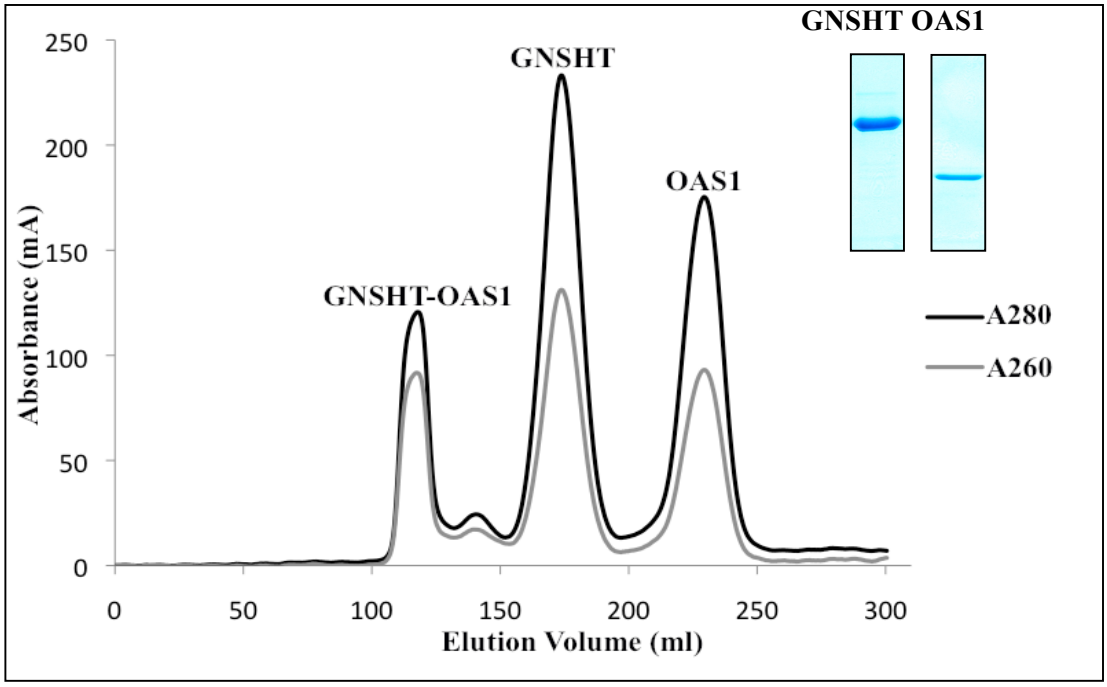

SEC purification of OAS1 was performed on HiLoad Superdex 200 26/60 at 3 ml/min and eluted with storage buffer (50 mM Tris-HCl, 100 mM NaCl, and 1 mM DTT, pH 7.5). UV readings were recorded at both 280 and 260 nm. Fractions from each peak were checked by 8% SDS-PAGE as previously described, and partial SDS-PAGE results are shown in the inset.

2.2.2.5 Confirmation of OAS1 by mass spectrometry

Purified OAS1 protein was excised from SDS-PAGE gels. In-gel reduction, alkylation and destaining were performed as described previously (106). Peptide mixture (0.5 µl) was mixed with DHB matrix solution (0.5 µL, saturated 2,5-dihydroxybenzoic acid in 2% formic acid, 25% acetonitrile) on a MALDI target. Spectra were obtained on a MALDI time-of-flight instrument (107). The accumulated peak list was sent to MASCOT (www.matrixscience.com), and putative OAS1 peptides were then analyzed by tandem mass spectrometry on the same instrument (108).

2.3 *In vitro* transcription and purification of VA_I RNA

2.3.1 Overview

For biochemical and structural studies of RNA-protein interactions, milligrams of high quality RNA are required. In general, two RNA synthesis methods are used conventionally: chemical synthesis and *in vitro* transcription by bacteriophage T7 RNA polymerase. RNA chemical synthesis is expensive and is not suitable for synthesizing long RNA (>50 nt) (109). For longer RNAs (>50 nt), *in vitro* transcription by T7 polymerase is employed (110). In this method, RNAs are transcribed from linearized DNA templates by T7 polymerase under the optimized conditions, including Mg^{2+} and nucleotide triphosphate (NTP) concentrations (111). T7 polymerase is readily expressed and purified from *E. coli* cells in house and stored in a suitable buffer at -20°C for weeks. For transcription of longer RNAs, the DNA templates can be synthesized biochemically as linearized plasmids. After transcription by T7 polymerase, RNAs are not fully pure to be used for further biochemical or structural experiments. In the initial transcribed RNA

samples, there are several impurities present: abortive transcripts, premature termination products, hydrolyzed RNA products, DNA templates, excessive NTPs and T7 polymerase. In order to purify RNAs from these impurities, preparative gel electrophoresis has traditionally been used (112). Two major drawbacks limit the application of these methods in the large-scale production of RNAs. One is the limiting sample loading volume in the gel. The other is the gel components associated with RNA representing further impurities (111). Fast-performance liquid chromatography (FPLC) has been used as a standard method to purify large amounts of macro-biomolecules, such as proteins and nucleic acids (113). By FPLC, the RNA of interest is separated from other impurities based on their hydrodynamic size. RNA transcription from a DNA plasmid together with FPLC, therefore, provides a fast, large-scale method to prepare longer RNA materials for structural biology study. In my thesis work, a DNA template-based *in vitro* RNA transcription and purification procedure was employed (114). This procedure includes the following steps: DNA template preparation, *in vitro* transcription, phenol/chloroform extraction, desalting of *in vitro* transcribed RNA, FPLC size-exclusion chromatography, RNA concentration and quality control assay, and storage (114, 115) (**Fig.10**). Specifics of each step will be outlined in the following section (2.3.2).

Figure 10 ***In vitro*** **RNA transcription and purification**

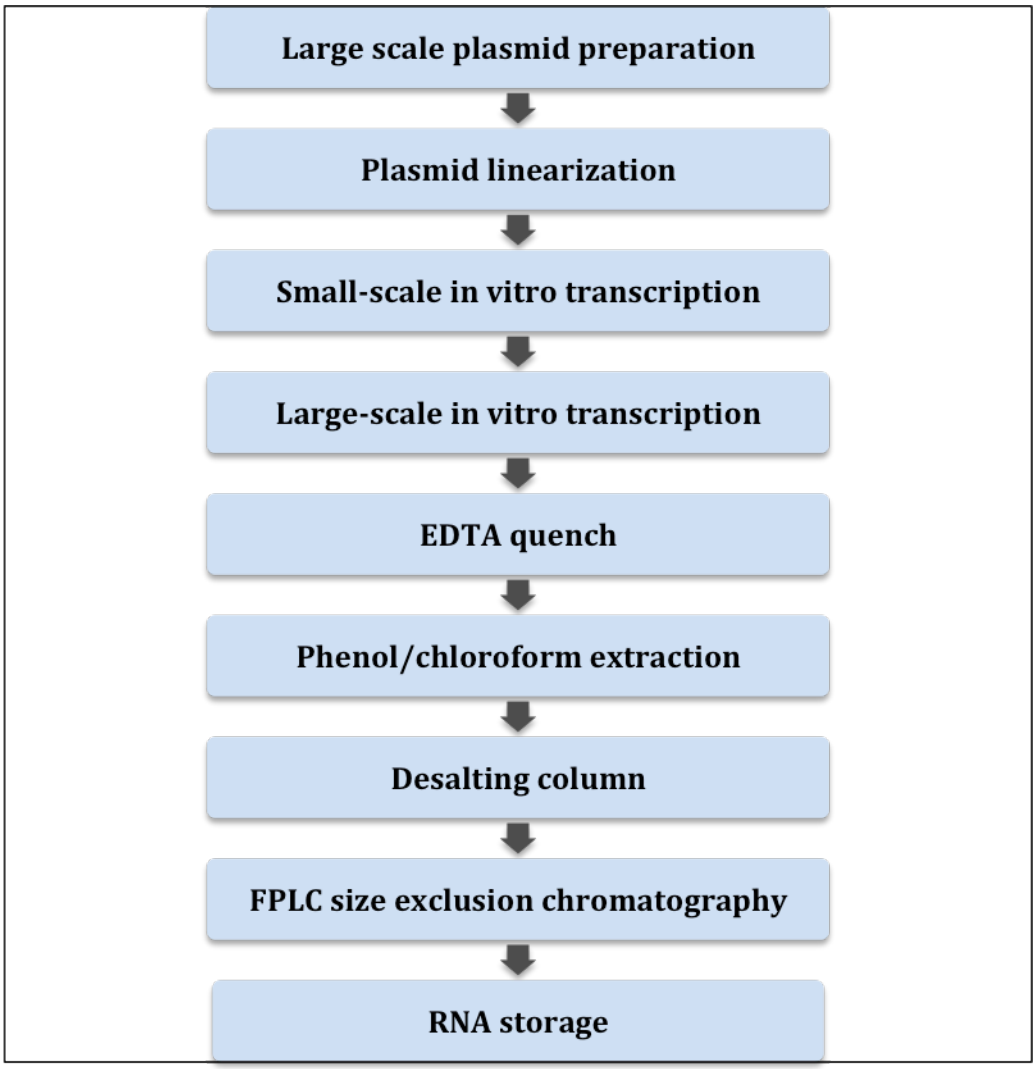

Schematic outline of in vitro RNA transcription and purification steps. Details of each step are described in sections (2.3.2).

2.3.2 Procedures

2.3.2.1 Preparation of DNA templates and *in vitro* transcription

A large-scale and non-denaturing approach was employed to generate VA_I RNA and its truncated derivatives, $VA_I\Delta TS$, VA_I-AS and VA_I-CS *in vitro*. Their sequences and secondary structures are illustrated in **Fig.5**. Briefly, the DNA templates used for *in vitro* transcription were purified following the Zyppy™Plasmid Maxiprep protocol (ZYMO RESEARCH), and linearized by incubating with *Bsa*I or *Bst*z17I at 37°C overnight. The linearized DNA templates were precipitated with 3 M sodium acetate and a four-fold excess of cold ethanol, and pelleted by centrifugation. The DNA pellet was dissolved in HPLC-grade water to a final concentration of 500 μg/ml. The small-scale trial transcriptions were required to optimize reaction conditions, especially the amount of T7 RNA polymerase and the concentrations of $MgCl_2$. A typical small-scale reaction contained the following: 1x transcription buffer (40 mM Tris-HCl (pH8.1), 1 mM spermidine, 0.001% (wt/vol) Triton X-100 and 10 mM DTT in HPLC water), 8 mM NTPs (ATP, GTP, CTP, UTP, 2 mM each), 2.5 μg linearized DNA template, varying concentrations of $MgCl_2$ (ranging between 5 and 20 mM in 5 mM increments), and 0.5, 1.0 or 2.0 μl of T7 RNA polymerase. The trial reactions were incubated at 37°C for 1-2 h, and 10-μl aliquots were assayed by denaturing TBE-PAGE. For denaturing TBE-PAGE, the gel mixture contained 8 M Urea to denature secondary RNA structures. RNA samples were mixed with denaturing loading buffer [0.02% bromophenol blue, 0.01% xylene cyanol FF, 10% glycerol, 8 M Urea in 1×TBE (89 mM Tris, 89 mM Boric acid, 2 mM EDTA, pH at 25°C: 8.0)] and preheated at 95°C for 5 min. After loading, the gels

were run at 100 V for 1-2 hr in 1×TBE, stained in 0.1% toluidine blue solution for 5 min, and then destained in water to visualize the RNA bands. After optimizing the reaction conditions, the small-scale transcriptions were scaled up to the desired size, and the large-scale transcriptions were incubated for 3-4 h at 37°C. Following removal of the pyrophosphate precipitate by centrifugation, the transcription reaction was quenched by adding excess EDTA to a final concentration of 50 mM to chelate the remaining Mg^{2+}. An equal volume of phenol/chloroform (1:1) was added to the quenched reaction to remove the restriction enzyme (*Bsa*I or *Bst*z17I) and T7 RNA polymerase.

2.3.2.2 Desalting of *in vitro* transcribed RNA

The phenol/chloroform treated transcription reaction was run through a 10-DG desalting column (BioRad Inc.) to remove the trace phenol/chloroform and significant amounts of DNA template and small molecule contaminants (including salt ions and NTPs). The 10-DG column was equilibrated with 20 ml RNA buffer (50 mM Tris-HCl, pH7.5, 100 mM NaCl). A 3-ml volume of phenol/chloroform treated transcription reaction was loaded onto the column and drained. The desired RNA transcript was eluted from the column by using 5 ml RNA Buffer. Columns were washed with the same buffer and reused until the entire large-scale transcription reaction had been desalted.

2.3.2.3 Purification of transcribed RNA using FPLC size exclusion chromatography

The desired RNA transcript fractions from the 10-DG column were further purified by FPLC size exclusion chromatography to remove the remaining DNA templates, abortive transcripts and NTPs. The FPLC system we employ is the ÄKTA Purifier 10 system with a Fac-950 fraction collector and a computer running the UNICORN 6 control software (GE Healthcare). The desalted RNA transcripts were

injected onto the size exclusion column via a 50-ml Superloop. Following injection, the RNA transcript was eluted from the column by RNA buffer at a constant rate of 2 ml/min, and the desired RNA fractions were collected (5 ml/fraction). The fractions containing the RNA of interest were confirmed by both denaturing and non-denaturing TBE-PAGE. Denaturing TBE-PAGE was performed as described earlier (Section 2.3.2.1). In the case of non-denaturing TBE-PAGE, electrophoresis was performed in 0.5 × TBE at 70 V, 4°C, and then the gel was stained by SybrGreen II (Invitrogen Inc.).

2.4 OAS1 activity assay

2.4.1 Overview

OAS enzyme activity has been monitored by several different methods. Traditionally, enzymatic activity of OAS enzymes was examined by direct detection of isotope-labeled 2'-5'-A using radioactive (^{32}P) ATP as reaction substrates (116). After incubation of OAS enzyme with dsRNA and ATP, the resultant 2'-5'-A are analyzed by thin-layer chromatography (TLC), PAGE, or high performance liquid chromatography (HPLC) to identify different forms of 2'-5'-A containing ^{32}P (117-121). Some effort has been made to develop nonradioactive methods to measure OAS activity. In this case, the detected product is inorganic pyrophosphate (PPi) generated during the production of 2'-5'-A by OAS enzymes. It has been reported that equal molar NADPH generated from PPi via an enzyme-coupled reaction has strong fluorescence, which can be measured spectrophotometrically (60, 122). The enzyme-coupled reaction involves three enzymes: UDP-Glc pyrophospharylase, phosphoglucomutase and glucose-6-phosphate dehydrogenase (122). The drawback of this assay is the involvement of a multistep

enzyme reaction, which prolongs the protocol and increases its complexity. In this thesis, a more direct colorimetric assay has been employed to measure PPi generated by OAS1. PPi reacts with ammonium molybdate to form PPi-molybdate complexes in sulfuric acid. PPi-molybdate complexes develop a blue color in the presence of thio reagent (β-mercaptoethonal) and a developing reagent (Eikonogen) (123) (**Fig.11**). The color change results in an absorbance maximum at 580 nm. This assay does not involve any additional enzymatic components and is sensitive up to 20 nmoles in a 1-ml reaction volume. Another advantage of this assay is the timesaving feature. It only takes 2 to 3 hours to finish the entire process as opposed to radioactive assay (usually one day).

Figure 11 OAS activity assay outline

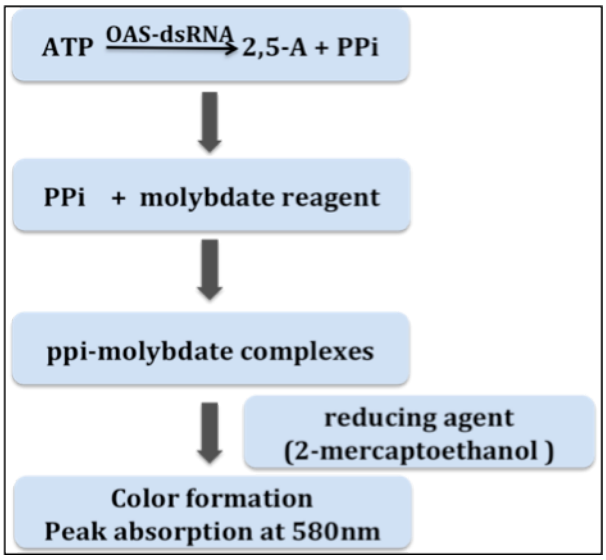

PPi reacts with ammonium molybdate to form PPi-molybdate complexes in sulfuric acid. PPi-molybdate complexes develop a blue color in the presence of thio reagent (BME) and a developing reagent (Eikonogen) (123). The color change results on an absorbance maximum at 580 nm.

2.4.2 Procedures

A colorimetric method was developed to quantitate the amount of PP_i product released upon the formation of 2'-5'-A by OAS1, modified from previously established assays (123, 124). OAS1 and RNA were incubated in the presence of 20 mM Tris-HCl, 5 mM $MgCl_2$, 1 mM DTT and 2 mM ATP in total volume of 100 µL at 37°C, and the reaction quenched at specific time points by the addition of 50 mM EDTA. A 100-µl aliquot of molybdate reagent (2.5% ammonium molybdate in 2.5 M H_2SO_4) and 100 µl of β-mercaptoethanol (BME) (0.5M) were added to the quenched reaction mixture to produce molybdophosphoric acid. To this mixture 40 µl of Eikonogen reagent (0.125 g of 1-amino-2-naphthol-4-sulfonic acid, 0.125 g of sodium sulfite, and 7.325 g of sodium bisulfite to 100 mL of ddH_2O) was immediately added and the final volume was adjusted to 1 ml with ddH_2O. The resulting molybdenum blue chromophore produced was then quantified by A_{580nm} measurement, and compared to PP_i standard solutions subjected to an identical process. Kinetic analysis used identical reaction conditions and followed a data analysis approach as outlined previously (60). Briefly, reaction velocities (V) were calculated by linear regression within the linear range of time course, ensuring that results were obtained in at least triplicate prior to analysis. The apparent dissociation constant (K_{app}) and the maximum reaction velocity (V_{max}) were determined using the following equation: $V = (V_{max} /1+ K_{app} /[RNA])$ (Kaleidagraph, from Synergy Software) (60). Curves were fit using non-linear regression and the quality of the fit assessed by examination of the R_{fit}.

2.5 Electrophoretic mobility shift assays

OAS enzyme and VA_I RNA were incubated in binding buffer (50 mM Tris-HCl, pH 7.5, 100 mM NaCl) at room temperature for 15 min. The reactions were mixed with native load mix (0.02% bromophenol blue, 0.01% xylene cyanol FF, 10% glycerol in 1×TBE), and loaded onto a native TBE-PAGE gel. Electrophoresis was performed at 70 V and 4°C. in 0.5×TBE for 3-4 hrs. To visualize RNA-containing species, gels were stained with SybrGreen II (Invitrogen Inc.) and imaged by FluorChem Q System (ProteinSimple, Inc.). Dissociation constant determination was performed according to the methodology outlined by Ryder *et. al* (125). The fraction of bound RNA (*f)* is related to the dissociation constant (K_d) by the following equation: $f = 1/1+(K_d/[P_t])$, wherein P_t is the total protein concentration at equilibrium. By determining *f* values at multiple OAS1 concentrations, K_d at equilibrium was derived from a nonlinear least-squares fit (125). *f* values were determined by AlphaView® Q software (ProteinSimple).

2.6 Hydrodynamic radius determination

Dynamic light scattering profiles were measured using the Zetasizer Nano S system (Malvern Instruments Ltd., Malvern, UK). RNA and protein preparations were passed through a 0.1 μm filter (Millipore) before dilution and allowed to equilibrate to 20 °C prior to DLS measurements at the same temperature. Multiple dataset replicates were analyzed using the DTS software supplied by the manufacturer (version 5.10.2). The obtained diffusion coefficient (and calculated hydrodynamic radius) was corrected to standard solvent conditions.

2.7 Mass spectrometry analysis of protein-RNA complexes

Aliquots of pure protein or protein-RNA mixtures were pipetted into Slide-A-Lyzer units (Pierce) and dialyzed overnight against ammonium acetate buffer (99.999% Aldrich) (126). In some cases, some of the sample was removed, and the dialysis continued against a lower concentration of buffer. Actual buffer concentration ranged from 5 to 100 mM. Samples were diluted to approximately 1 μM, inserted into a New Objective PicoTip™, then analyzed on an electrospray time-of-flight instrument (127). The declustering voltage was varied in order to determine the relative stability of the complexes. Attempts to denature samples with acetic acid and methanol resulted in protein precipitation, and therefore we were unable to measure the protein in the unfolded state.

2.8 5'-end modification of RNA

Plasmid-based in vitro transcription of RNAs generates 5'-triphosphates (5'-PPP) under standard conditions. To generate a fully dephosphorylated 5'-ends (5'-OH), a 500-μl reaction containing purified RNA (50 μg) was treated with calf intestinal alkaline phosphatase (50U, New England Biolabs) in 1×NEBuffer3. To generate a 5'-monophosphate (5'-P), RNA (50 μg) was instead treated with RNA 5' Pyrophosphohydrolase (50U, New England Biolabs) in 1×NEBuffer2. Reactions were incubated at 37 °C for 90 minutes, followed by repurification as described in section 2.3.2 using phenol/chloroform extraction, a 10-DG desalting column, and FPLC to

remove the modifying enzyme and reaction components. Confirmation that the RNA remained intact was confirmed by both denaturing and non-denaturing TBE-PAGE.

Chapter 3

Results

3.1 Introduction

Our main goal was to characterize the ability of VA_I RNA and its derivatives to regulate the activity of a key interferon-inducible member of the innate immune response, OAS1. A single study has demonstrated that full-length VA_I RNA activates the murine OAS enzyme, which is paradoxical given the inhibitory role that VA_I RNA plays with respect to PKR (42, 80). VA_I RNA binds to PKR and prevents the required self-association of PKR for activation (40). Recent investigations suggested that VA_I RNA is processed by Dicer into two species: a TS-lacking VA_I RNA and small RNA from TS *in vivo* (84). Further, TS-lacking VA_I RNA that corresponds to the Dicer-processed version (VA_I ΔTS) has been demonstrated to still serve as an inhibitor for PKR (128). In light of the discovery that Dicer efficiently truncates VA_I, we decided to investigate the regulation of the specific OAS1 isoform (p42) by both the full-length VA_I and its truncated derivatives, including VA_I ΔTS. Using a combination of biochemical approaches, we characterized both RNA-protein complex formation and activation/inhibition potential of these RNA molecules. Additionally, the importance of RNA 5'-end phosphorylation state to its ability to regulate OAS1 activity has been investigated. Detailed results will be discussed in the sections 3.2-3.6.

3.2 Expression and purification of active OAS1 from *E. coli*

Studies with purified OAS1 protein have been difficult because of yield and solubility problems, so we developed a new preparation method in which recombinant OAS1 is purified from *E. coli* as a fusion protein with highly soluble bacterial protein domains. Cleavage of the fusion tag results in a monomeric 42 kDa protein by denaturing SDS-PAGE (**Fig.12a**), and analysis of the trypsinized protein by MS confirmed OAS1 purification (data not shown). To test catalytic activity, a novel colorimetric assay was developed which correlates the detection of PP_i with the production of 2'-5'-A chains. We prepared buffered reactions containing OAS1, ATP and $MgCl_2$ in in the presence and absence of a known synthetic dsRNA activator (poly I:C), and 2'-5'-A synthesis was determined by detection of PP_i production after incubation at 37 °C (**Fig.12b**). In the absence of activator, no detectable catalytic activity is observed, whereas in the presence of poly I:C, catalysis of 2'-5'-A chain formation is significantly enhanced at all time points examined, consistent with an active enzyme. To ensure that the activity of the purified recombinant OAS1 was consistent with previously reported values (60), kinetic experiments were performed in which increasing concentrations of activator (poly I:C) were incubated in the presence of OAS1, and PPi production determined at various time points. From the linear phase of these data, reaction velocities (V) were calculated, and plotted against poly I:C concentration in order to extract kinetic parameters (**Fig.12c**). The analysis was repeated at multiple OAS1 concentrations (50-400 nM), and determined an apparent dissociation constant (K_{app}) of 17$\pm$3 μg/mL, and a maximum reaction velocity (V_{max}) of 2.07$\pm$0.06 nmol/min. These results are consistent with previously reported values of K_{app} (42 μg/mL) and V_{max} (1.29 nmol/min) (60).

Figure 12 Purification of active recombinant human OAS1

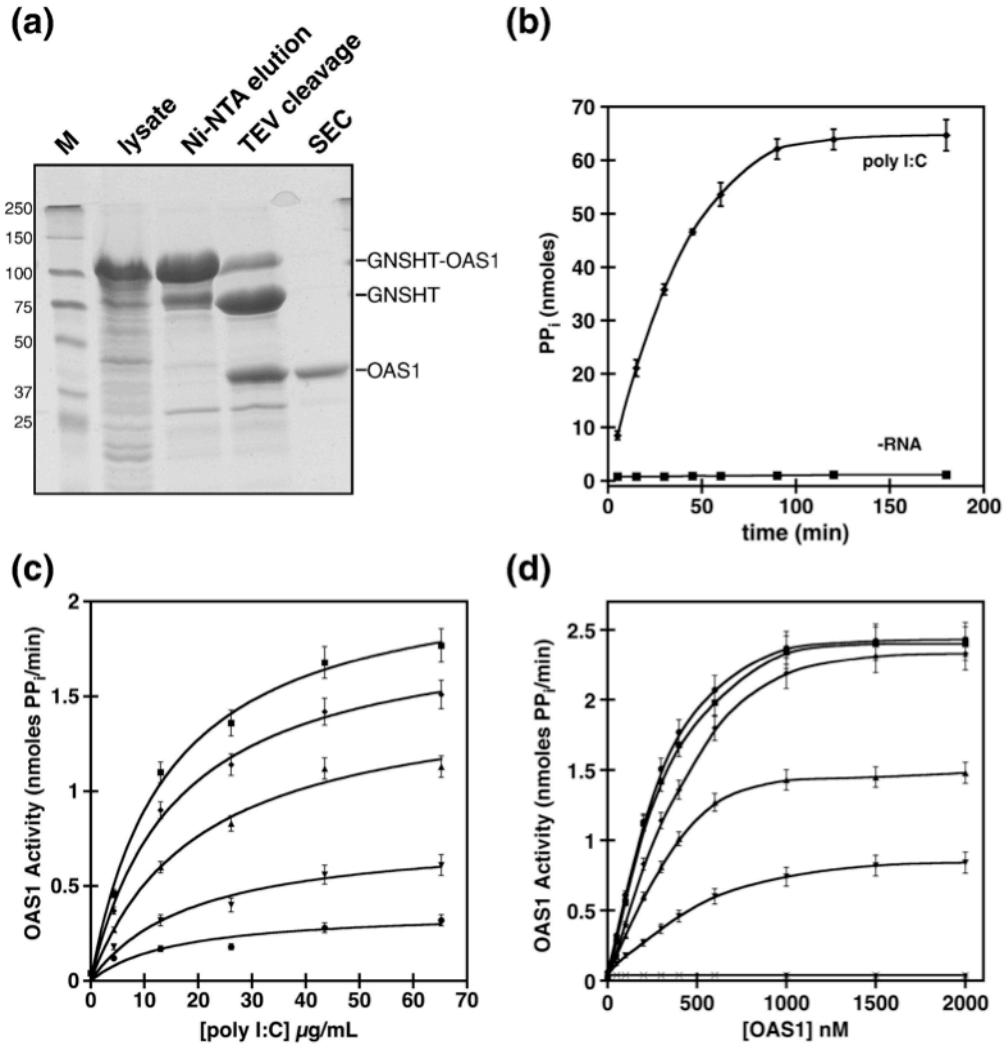

(a) Denaturing SDS-PAGE analysis of OAS1 purification from *E. coli*. Lanes correspond to (left to right) molecular weight markers, lysate following sonication, the imidazole eluate from Ni-NTA affinity chromatography, cleavage of the fusion protein with TEV protease, and purified protein following size exclusion chromatography. The migration of fusion protein (GNSHT-OAS1), the cleaved affinity tag (GNSHT), and pure OAS1 protein are indicated. **To be continued in next page.**

(b) Purified OAS1 (300 nM) and polyI:C (20 µg/mL) were incubated in the presence of ATP (2mM) and $MgCl_2$ (5 mM) at 37°C and quenched at time points from 0-180 minutes to assay 2-5(A) chain formation. Errors represent the standard deviation from 3 replicates. **(c)** Enzymatic activity (V_o) is shown as a function of poly I:C concentration for OAS1 at 50 nM (**l**), 100 nM (▼), 200 nM (▲), 300 nM (**u**), and 400 nM (**n**) after 20 minute incubation. Higher concentrations were sampled, but the data was excluded as a result of poor fit as described in the Materials and Methods. Error bars reflect the error in the linear regression analysis in order to determine *V*. **(d)** Identical experiments as in (C) were performed, demonstrating the linearity of the assay with respect to enzyme concentration at low enzyme concentrations. Reaction velocity (*V*) is shown as a function of OAS1 concentration for poly I:C RNA at 0 µg/mL (x), 4.3 µg/mL (▼), 13.0 µg/mL (▲), 26.1 µg/mL (**u**), 43.5 µg/mL (**n**), and 65.2 µg/mL (**l**) after 20 minute incubation. Error bars reflect the error in the linear regression analysis in order to determine *V*.

Upon correcting for enzyme concentration used, a turnover number (k_{cat}) of 69$\pm$9 min^{-1} was determined for our preparation as compared to a value of 108 min^{-1} reported previously. To ensure that enzymatic assays were being performed at appropriate OAS1 concentrations, the linearity of the assay was established by titrating different concentrations of protein at a fixed RNA concentration and time point (**Fig.12d**). For a given RNA concentration, the assay responds linearly to enzyme concentration at lower OAS1 concentrations, eventually resulting in saturation of activity when excess OAS1 is

added. As a result, we have confined activation assays to enzyme and RNA concentrations within the linear range in future experiments.

3.3 VA_I lacking the terminal stem forms stable complexes with OAS1

To characterize the interaction between VA_I RNA and OAS1, we produced four distinct RNA molecules to probe the regions responsible for interaction (**Fig.5**). In addition to full-length VA_I, the central stem alone (VA_I-CS), the apical stem alone (VA_I-AS), and a mimic of Dicer-processed VA_I lacking the terminal stem ($VA_I\Delta TS$) were examined. EMSA under non-denaturing conditions was used to probe the affinity of OAS1 for each RNA molecule. Under conditions of a 4-fold molar excess of RNA relative to protein, $VA_I\Delta TS$ was capable of the most significant complex formation with OAS1 (**Fig.13a**). VA_I-OAS1 and VA_I-CS-OAS1 complexes were also observed, whereas no detectable complex formation occurred with the apical stem alone at the concentrations examined. Quantitative comparison of binding affinities of full-length VA_I and $VA_I\Delta TS$ for OAS1 was performed by full titration of RNA with increasing amounts of OAS1. $VA_I\Delta TS$ demonstrated the highest affinity, with conversion of the free RNA into two distinct higher molecular weight complexes (**Fig.13b**). An apparent dissociation constant (K_D) based on the quantitation of free RNA disappearance was determined to be 590±40 nM (**Fig.13c**). A 2.7-fold lower binding affinity (1610±80 nM) was determined when a similar analysis was performed with full-length VA_I.

Figure 13 VA_I lacking the terminal stem forms stable complexes with OAS1

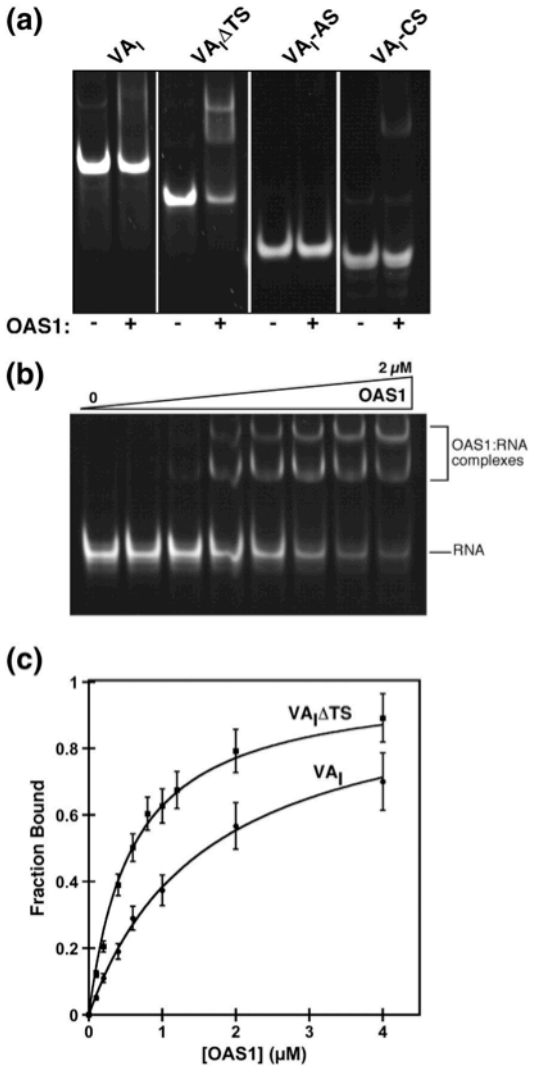

(a) EMSA for OAS1 (800 nM) binding to VA_I RNAs (200 nM) under non-denaturing conditions. **(b)** EMSA for OAS1 binding to $VA_I\Delta TS$ (50 nM). Increasing amounts of OAS1 were added from 0-2 μM. **(c)** Quantitation of EMSA results for $VA_I\Delta TS$ (squares) and full length VA_I (circles). Experiments were repeated in triplicate, with associated standard deviation indicated as error bars. Dissociation constant determination was performed according to the methodology outlined by Ryder *et. al.* (125).

Figure 14 Characterization of VA_I:OAS1 by DLS

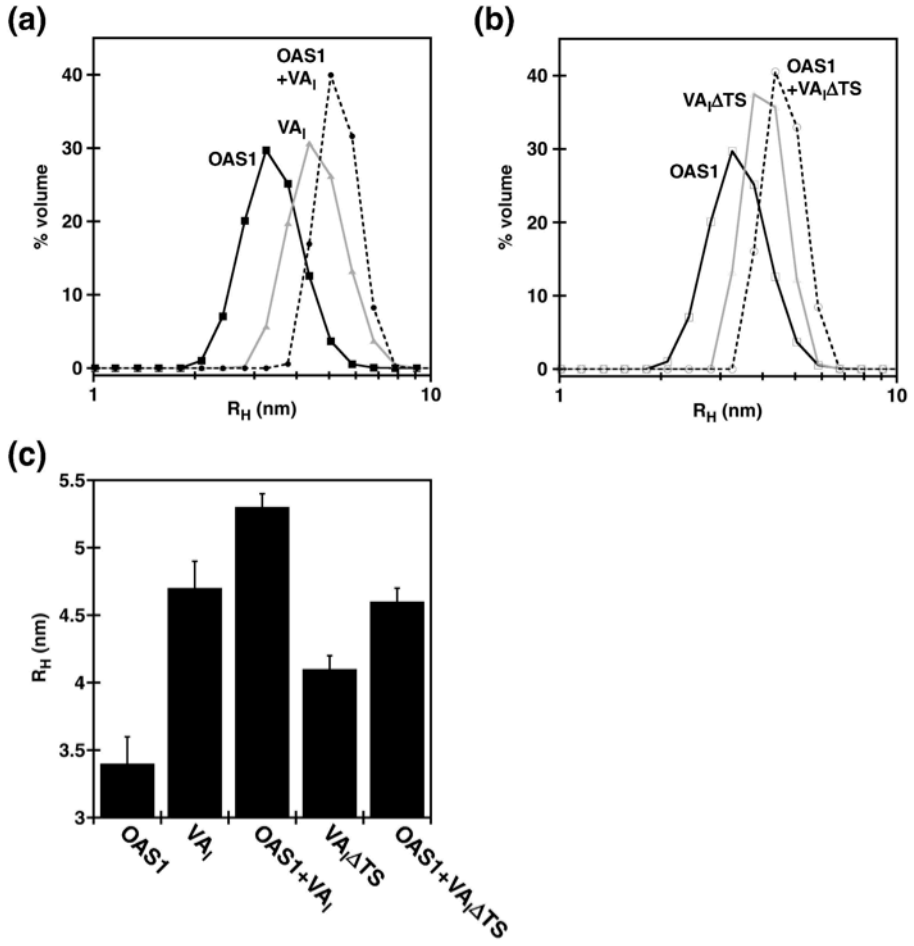

Hydrodynamic radius (R_H) determination of **(a)** OAS1-VA_I complex and individual components and **(b)** OAS1-VA_IΔTS and individual components by DLS. OAS1 (8 μM) and RNA (2 μM) were mixed, purified, and equilibrated to 20 °C in the cuvette prior to acquisition. **(c)** Quantitation of DLS experiments as outlined in **(a)** and **(b)**. Error bars represent the standard deviation from triplicate experiments.

To characterize the observed complexes, we subjected VA_I-OAS1 and $VA_I\Delta TS$-OAS1 complexes to DLS analysis to determine complex size and polydispersity. Given that DLS requires significantly higher concentrations than EMSA approaches, this technique can also rule out the possibility that higher-order complexes were formed but not observed by EMSA. As comparison points, the hydrodynamic radii (R_H) of OAS1 (3.4±0.2 nm), VA_I (4.7±0.2 nm), and $VA_I\Delta TS$ (4.1±0.1 nm) were determined (**Fig.14**). As expected, clear increases in R_H to 5.3±0.1 nm and 4.6±0.1 nm are observed upon OAS1 complex formation with VA_I and $VA_I\Delta TS$ respectively (**Fig.14**). Both VA_I and $VA_I\Delta TS$-containing complexes had less than 20% polydispersity, indicating a fairly uniform complex size.

3.4 Non-denaturing mass spectrometry of $VA_I\Delta TS$-OAS1 complex

EMSA results suggested that VA_I lacking the terminal stem forms two higher molecular weight complexes with OAS1. To determine the stoichiometry of these complexes, we characterized complexes using non-denaturing MS in positive mode. By manipulation of the buffer concentration, the relative concentrations of the two components, and the declustering voltage in the mass spectrometer, we were able to identify all components. OAS1 demonstrated the properties of a stable, well-folded, monomeric protein as only 4 charge states were observed (+11 to +14) (**Fig.15a**). Spectrum deconvolution identifies 4 major protein peaks starting at 42096 Da (calculated mass of 42100 Da) and each separated by 76 Da. Given that 76.01 Da corresponds to the mass of BME, the original reducing agent used in our OAS1 preparation, it was not

surprising that upon tryptic digest of the protein, the MALDI mass spectrum showed three pairs of ions separated by 76 Da. Tandem ms of these pairs identified three cysteines that had been covalently modified by BME which accounts for the multiple species in the deconvolution. The protein subsequently prepared using DTT as the reducing agent had one protein species of 42096 ± 5 Da and had no modifications (data not shown). Effects by BME covalent modification on complex formation was also demonstrated by EMSA results (**Fig.16**). When using BME for OAS1 purification, a single shifted complex was observed by EMSA (**Fig.16a**). When DTT was used instead of BME, two shifted complexes were observed by EMSA (**Fig.16b**). Analysis of the RNA component alone, $VA_I\Delta TS$, proved problematic as it was not possible to run the sample in negative mode in the absence of OAS1. To circumvent this issue, we made a sample containing OAS1 with excess $VA_I\Delta TS$ and adjusted to desclutering voltage such that only free RNA signal was detected. $VA_I\Delta TS$ shows a single ion envelope with four charge states (9+ to 12+) consistent with a well-folded nucleic acid molecule (**Fig.15b**).

To probe complex stoichiometry, the nanospray spectrum of OAS1-$VA_I\Delta TS$ complexes were generated from protein prepared with DTT as the reducing agent (**Fig.15c**). Given that the best spectra for OAS1 protein by itself were obtained with both high buffer concentration and high declustering voltage, while the best $VA_I\Delta TS$ spectra had the opposite requirements, a wide range of both parameters were tested in order to maximize the trade-off between resolution and maintenance of the non-covalent complex. Under the best compromise, four distinct charge envelopes were observed. The most prominent charge envelope (8+ to 11+ ions) exactly matches that observed for the free $VA_I\Delta TS$ shown in Figure 5B. More importantly, there are charge envelopes

corresponding to two distinct OAS1-$VA_I\Delta TS$ complexes; a prominent envelope (19+ to 25+) corresponding to a complex of 120356±166 Da and a subtle envelope (16+ to 18+) of a species with an average mass of approximately 78 kDa. Using the established molecular masses from OAS1 and $VA_I\Delta TS$ alone (**Figs.15a and 15b**), these measurements correspond to 2:1 and 1:1 OAS1:$VA_I\Delta TS$ complexes. A distinct charge envelope corresponding to free OAS1 (14+ to 16+) is present, but the higher charge states indicate partial unfolding (compare to **Fig.15a**). At 120 V declustering voltage, these ions were visible, and thus may represent a small amount of unfolded protein. As the voltage was increased, there was an increased abundance of the "unfolded protein" ions and the ions from the species of mass 78 kDa appeared, suggesting fragmentation of the 2:1 complex during the ionization/desolvation stage in the mass spectrometer.

When OAS1 protein is prepared in the presence of DTT, two OAS1-$VA_I\Delta TS$ complexes are clearly detected by both EMSA and non-denaturing ms, while only the 1:1 complex is found when the protein is prepared in the presence of BME (**Fig.15d**). The well-defined charge envelope near *m/z* 3500 (11+ to 13+ ions) are the same as those shown in **Fig.15a** for OAS1 alone. The clear ions shown from *m/z* 4500 to 6000 (13+ to 16+) represent a species that corresponds well with a 1:1 stoichiometry. This result is particularly interesting in light of the observation that EMSAs with OAS1 purified in the presence of BME only form a single higher molecular weight complex as opposed to the two observed for protein purified using DTT (**Fig.15c**). It is important to note that the relative intensities of the charge states is a product of both affinity and declustering voltage selection, and therefore does not necessarily reflect abundance in solution; however, the spectra shown in **Figs. 15c** and **15d** were both generated with an

approximately equimolar mixture of protein and RNA, the major difference being the purification method used for the protein.

Figure 15 Non-denaturing MS of OAS1:VA_I TSΔ21 complexes

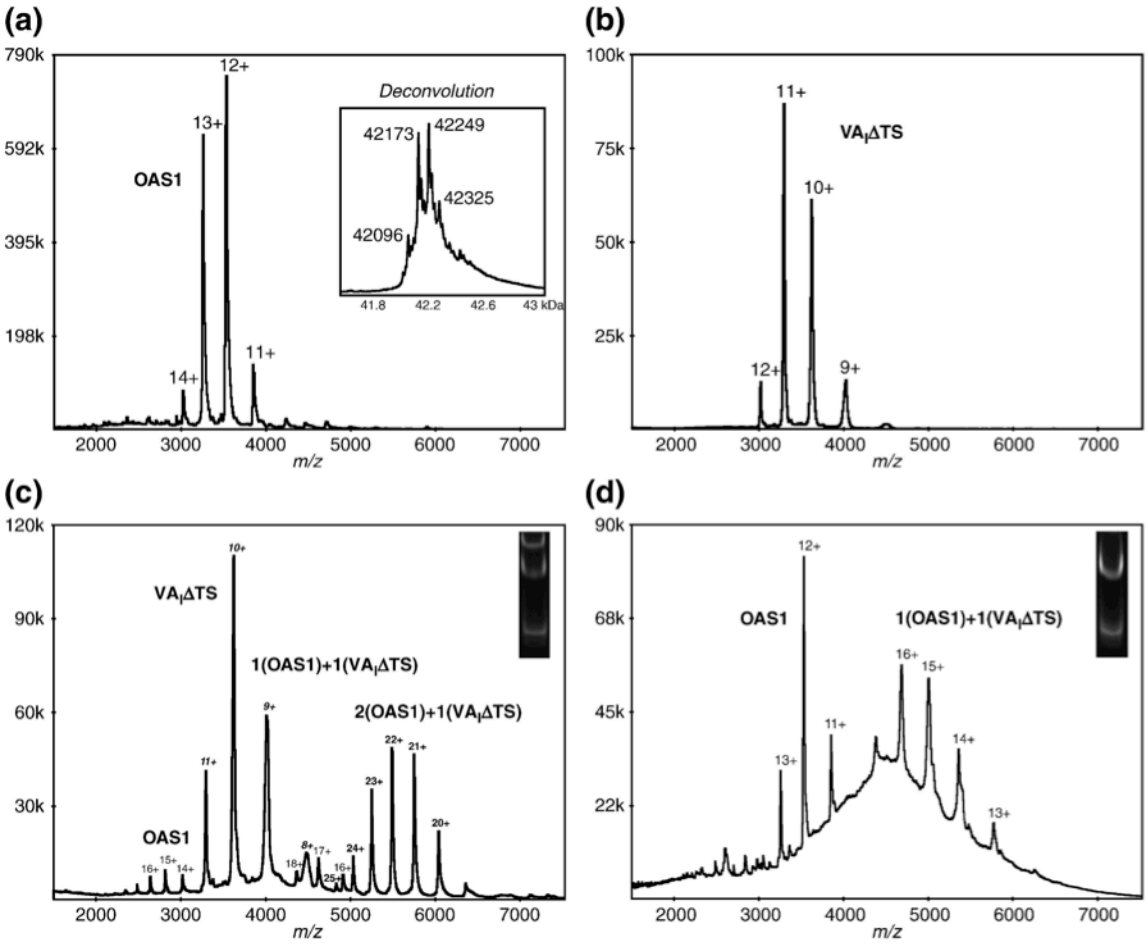

(a) Nanospray spectrum of OAS1 prepared in buffer containing BME and buffer-exchanged into 100 mM ammonium acetate. Declustering voltage was 280 V. Deconvolution shown in the inset gives at least four major protein masses (units: Da), each of which has multiple adducts. The major peaks differ by about 76 Da, the mass expected for a 2-ME addition, and the minor ones are sodium.

To be continued in next page.

(b) Nanospray spectrum showing $VA_I\Delta TS$ in 5 mM ammonium acetate with 150 V declustering voltage. Inset shows the deconvolution of the 9+ to 12+ ions. **(c)** Section of a nanospray spectrum of a mixture of OAS1 and $VA_I\Delta TS$ prepared in buffer (5 mM ammonium acetate) containing DTT. Declustering voltage was 180 V. There are two prominent charge envelopes labeled in bold type, the 8+ to 11+ ions that exactly match those of $VA_I\Delta TS$, and the 19+ to 25+ of a new species of mass 120356±166 Da (2:1 protein:RNA complex). Ions corresponding to OAS1 alone (14+ to 16+), and the 16+ to 18+ of a species of average mass 78291 Da are also indicated (1:1 protein:RNA complex). Non-denaturing EMSA of the mixture prior to ms analysis is inset. **(d)** Section of a nanospray spectrum of a mixture of $VA_I\Delta TS$ and OAS1 prepared in buffer (50 mM ammonium acetate) containing BME. Declustering voltage was 250 V. The ions labeled 11+, 12+ and 13+ have the same *m/z* values as the ions of the same charge state shown in (B) corresponding to OAS1. The clear ions from *m/z* 4500 to 6000 are the 13+ to 16+ of a species mass 74772 ±184 Da. Non-denaturing EMSA of the mixture prior to ms analysis is inset.

Figure 16 Effects of reducing agents on OAS1:VA$_I$ΔTS complex formation

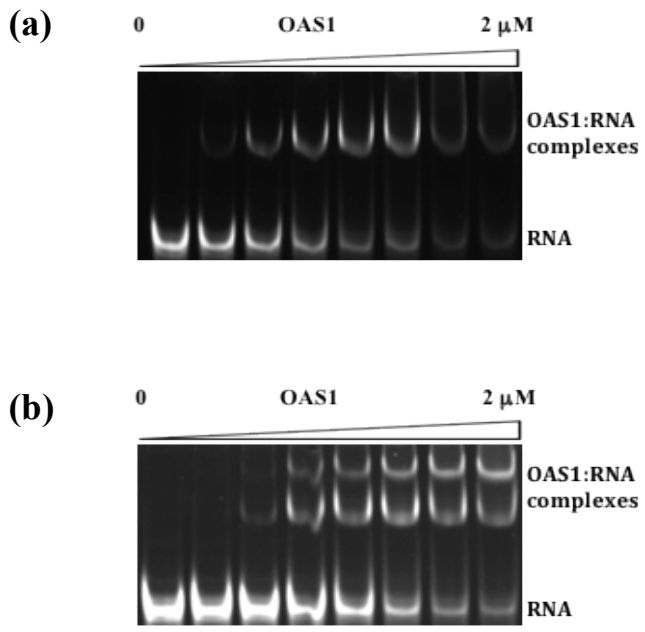

(**a**) EMSA for OAS1 (BME as reducing agent) to VA$_I$ΔTS (50 nM). Increasing amounts of OAS1 were added from 0-2 μM. (**b**) EMSA for OAS1 (DTT as reducing agent) to VA$_I$ΔTS (50 nM). Increasing amounts of OAS1 were added from 0-2 μM.

3.5 VA_I lacking terminal stem is a poor activator of OAS1

Once we had firmly established the affinity and stoichiometry of complex formation, we sought to characterize the ability of VA_I RNA to regulate the catalytic activity of OAS1. A novel colorimetric assay, which correlates the detection of pyrophosphate with the production of 2'-5'-A chains, greatly simplified this study. We prepared buffered reactions containing OAS1, ATP and $MgCl_2$ in the presence and absence of VA_I RNA derivatives, and monitored pyrophosphate production after a 30-minute incubation at 37 °C (**Fig.17a**). In the absence of RNA or in the presence of an ssRNA control, basal levels of OAS1 activity were detected. A significant enhancement in OAS1 activity was observed in the presence of full-length VA_I (6.3-fold) and VA_I-AS (11.3-fold), the most potent activators observed. VA_I-CS inclusion led to moderate OAS1 activation (3.3-fold). Surprisingly, VA_I lacking the terminal stem was the least effective activator of OAS1, leading to nearly basal levels of activation. It should be noted that all RNAs demonstrated significantly lower stimulation of activity than poly I:C on a per mass basis (**Fig.12b**), although direct comparison to poly I:C is problematic due to its large size and heterogeneity (~90-1400 kDa). A more comprehensive time course under similar reaction conditions was performed to ensure that the results were not biased by the particular time point being examined (**Fig.17b**). At all time points measured, a similar trend was observed: VA_I-AS was the most potent activator, followed by full-length VA_I, the central stem derivative, and finally $VA_I\Delta TS$ at levels approaching the negative control. Dose-response experiments in which OAS1-catayzed reaction velocities were determined under increasing RNA concentrations allowed estimation of the maximum reaction velocity (V_{max}) and apparent dissociation constant (K_{app}) (**Fig.17c**).

The results are summarized in **Table 1**, and support both the K_D values as determined by EMSA (**Fig.13c**) and the trend outlined from a single time course (**Fig.17b**). A 2.0-fold increase in affinity and 4.7-fold decrease in V_{max} were observed when comparing $VA_I\Delta TS$ to VA_I. Both K_{app} values are consistent with those determined by EMSA. VA_I-AS achieves the highest maximum reaction velocity despite a significantly lower affinity than other RNAs tested (K_{app}=2.4 μM). As expected, basal reaction velocities were observed when using an ssRNA control in the enzyme assay, although accurate parameter determination was not possible as a result of the high error associated with velocity estimations (reflected in the comparatively low R_{fit} value). poly I:C achieved a maximal velocity comparable with the most potent activator examined (VA_I-AS) and a significantly higher affinity than any VA_I derivative, although these values should be treated with caution as a direct comparison is clouded by the large size and heterogeneity of synthetic poly I:C.

To test our hypothesis that $VA_I\Delta TS$ was behaving as a pseudo-inhibitor, we established a competition experiment using a fixed concentration of the most potent activator, VA_I-AS, in the presence of increasing $VA_I\Delta TS$ (**Fig.17d**). As the concentration of $VA_I\Delta TS$ in the reaction mixture was increased, OAS1 activation was increasingly attenuated. Similar behavior was observed when using poly I:C as the activator, but quantitation of these results is again difficult due to the heterogeneity of poly I:C (data not shown). To ensure that these results were specific to $VA_I\Delta TS$, we repeated the experiment replacing $VA_I\Delta TS$ with an ssRNA control. Under these conditions, no significant reduction in OAS1 activation was observed.

Figure 17 Regulation of OAS1 activity by VA_I RNA

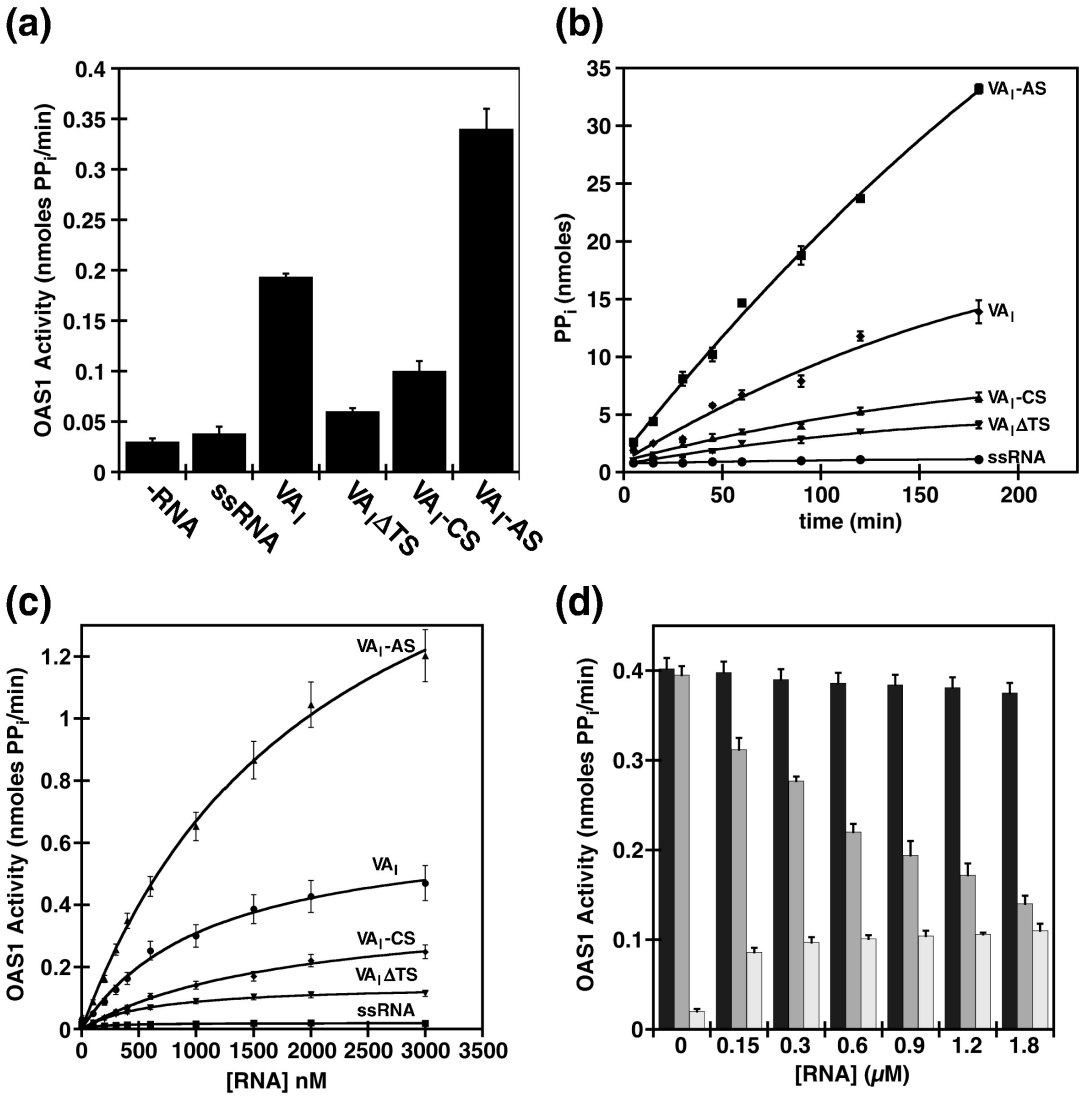

In all cases, errors represent the standard deviation from at least 3 replicates. **(a)** Purified OAS1 (300 nM) and VA_I derivatives (300 nM) were incubated in the presence of ATP (2mM) and $MgCl_2$ (5 mM) at 37°C for 30 minutes, quenched, and 2-5(A) chain formation quantitated by PP_i detection. **(b)** OAS1 catalytic activity was determined as in (a), with the exception that the reactions were quenched at time points from 0-180 minutes. A control with no RNA was also performed, but was not shown graphically as it overlapped the ssRNA control.

To be continued in next page.

(c) Enzymatic activity is shown as a function of RNA concentration for OAS1 (300 nM). Error bars reflect the error in the linear regression analysis in order to determine OAS1 activity. **(d)** Pseudo-inhibition of OAS1 activation by $VA_I\Delta TS$. OAS1 (300 nM) catalytic activity was determined in the presence of VA_I-AS (300 nM) under increasing concentrations of $VA_I\Delta TS$ (medium grey) or a ssRNA control (dark grey). The experiment was repeated with OAS1 (300 nM) in the presence of $VA_I\Delta TS$ alone (light grey) to establish baseline. OAS1 activity was determined after a 30 minute incubation at 37 °C.

Table 1 Estimated kinetic parameters for VA_I derivatives and controls

	K_{app} (nM)	V_{max} (nmol/min)	R_{fit}
VA_I	1348 ± 130	0.66 ± 0.03	0.996
$VA_I\Delta TS$	663 ± 65	0.14 ± 0.02	0.995
VA_I-AS	2403 ± 187	2.1 ± 0.1	0.996
VA_I-CS	1746 ± 222	0.40 ± 0.03	0.997
ssRNA	160 ± 84	0.02 ± 0.01	0.643
Poly I:C	92 ± 6	1.97 ± 0.05	0.997

Data from **Fig.17c** was fit as outlined in the Materials & Methods section to determine K_{app} and V_{max} values,. The quality of the fit is presented via the R_{fit} value, with a value of 1 representing a perfect fit. Values for poly I:C are denoted (*) as the molecular weight of poly I:C is heterogeneous (these numbers reflect an estimate based on an average molecular weight of 200 kDa).

3.6 RNA dissociation is observed upon OAS1 activation

To test the importance of a transient RNA-protein association to the mechanism of OAS1 activation, EMSAs were performed on $VA_I\Delta TS$ RNA in the presence of OAS1 under activating (ATP/Mg^{2+}) and non-activating (AMP/Mg^{2+}) conditions (**Fig.18a**). RNA is shifted to higher molecular weight in the presence of OAS1 alone. Addition of ATP/Mg^{2+} or AMP/Mg^{2+} resulted in identical migration when compared to OAS1 alone. Upon incubation at temperatures sufficient for OAS1 activation (90 minutes), dissociation of the OAS1-$VA_I\Delta TS$ complex is observed when both ATP and Mg^{2+} are present. Quantitation of these results indicated a 4.2-fold reduction in RNA association with OAS1 upon activation (**Fig.18b**). Similar observations were made for VA_I-AS, however the low intensity of the EMSA results precluded quantitative evaluation. When AMP is employed in place of ATP, no RNA dissociation is observed. This result suggests that upon formation of the catalytically active OAS1 complex, OAS1 behaves in an RNA-independent manner.

3.7 Phosphorylation state at RNA 5'-end impacts OAS1 affinity and activation potential

It has been proposed that a mechanism whereby the host cell can discriminate foreign viral dsRNA from self is at least partially based on the modification present at the 5'-end. Furthermore, Dicer processing of VA_I *in vivo* would typically result in a monophosphate group being left on the 5'-nucleotide of $VA_I\Delta TS$. We sought to determine the impact, if any, the phosphorylation state of the 5'-end had on the ability of

VA_I-derived RNAs to interact with and activate OAS1.

Figure 18 RNA affinity decreases upon even modest OAS1 activation

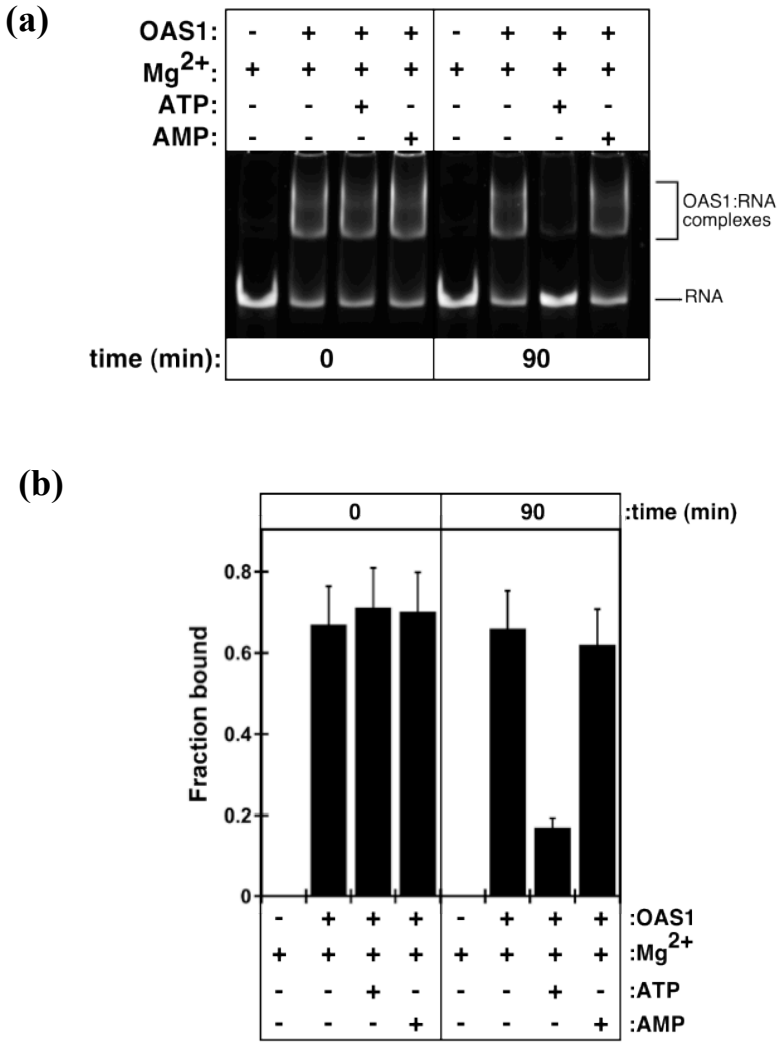

(a) Native gel mobility-shift for $VA_I\Delta TS$ (300 nM) binding to OAS1 (300 nM) in reactions containing ATP (2 mM) or AMP (2 mM) and $MgCl_2$ (5 mM). Samples were incubated for the time indicated, resolved on 5% TBE gel, and visualized by SybrGreenII staining. **(b)** Quantitation of triplicate experiments from (a), with error represented as standard deviation.

In vitro transcription of RNA generates molecules with 5'-triphosphates (5'-PPP) due to the use of nucleotide-5'-triphosphates in the reaction mixture. We used commercially available enzymes to generate the 5'-monophosphate (5'-P) and 5'-hydroxyl (5'-OH) versions of VA_I constructs and then repurified the RNAs to ensure that no residual enzyme or contaminants were present. Interestingly, alteration of $VA_I\Delta TS$ from a 5'-PPP to either a 5'-P or 5'-OH resulted in a greater than 60% decrease in activity (**Fig.19a**). A similar trend was observed for the most potent activator, VA_I-AS. To ensure that the treatment/purification of modified RNA did not contain residual enzymatic activity that could account for the data, identical assays were repeated with OAS1 omitted from the reaction mixture. Under these conditions, no significant change in PPi production was observed. OAS1 binding affinity to $VA_I\Delta TS$ was probed by EMSA and interestingly no significant decrease in affinity was observed when comparing the 5'-P to 5'-PPP derivative, although the 1:1 OAS1:RNA complex was not detected in the case of 5'-P (**Fig.19b**). A significant reduction in binding affinity was observed for the fully dephosphorylated RNA, indicating the potential importance of charge at the 5'-end.

3.8 Summary

By employing a combination of biochemical approaches, both VA_I RNA-OAS1 complex formation and OAS1 activation/inhibition potential of these RNA molecules have been investigated. Additionally, the importance of RNA 5'-end phosphorylation state to its ability to regulate OAS1 activity has also been investigated. Our results demonstrated that $VA_I\Delta TS$, the most physiologically relevant VA_I RNA derivative, serves as a pseudo-inhibitor for OAS1 enzyme.

Figure 19 5’-end phosphorylation impacts activity and affinity for OAS

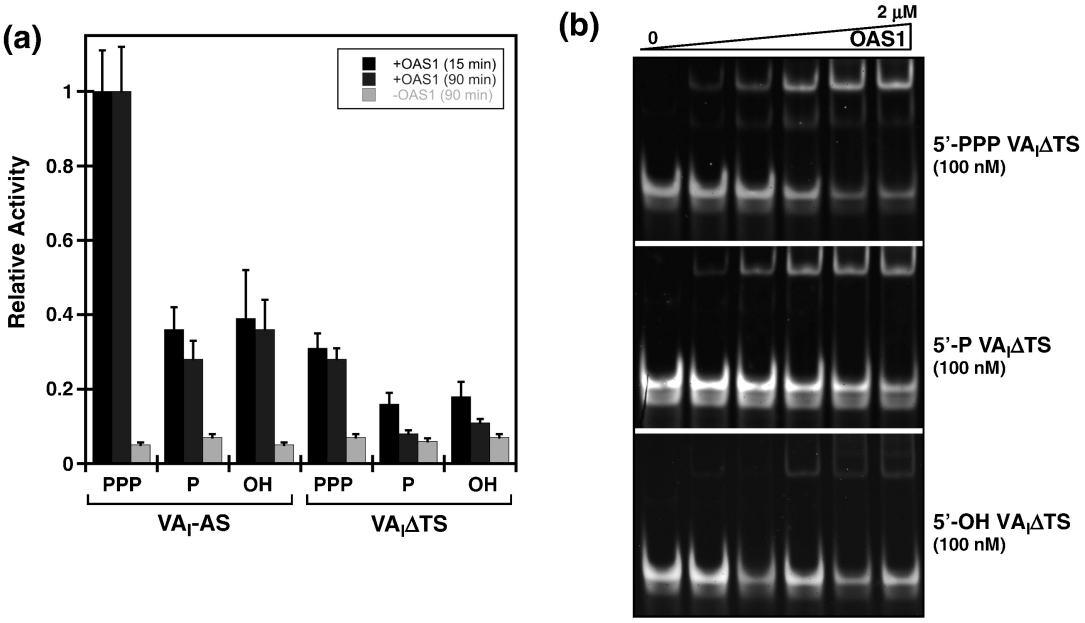

(a) Transcribed VA$_I$-AS and VA$_I$ΔTS containing 5’-triphosphates (5’-PPP) were enzymatically modified to form either 5’-monophosphate (5’-P) or completely dephosphorylated 5’-end (5’-OH) prior to purification by size exclusion chromatography. Purified OAS1 (300 nM) and RNA (300 nM) were incubated in the presence of ATP (2mM) and $MgCl_2$ (5 mM) at 37°C, quenched, and 2-5(A) chain formation quantitated by PP_i detection. As a control, reactions were repeated with OAS1 omitted. In all cases, errors represent the standard deviation from 3 replicates. **(b)** EMSA for OAS1 binding to VA$_I$ΔTS (100 nM) with various 5’-end phosphorylation states. Increasing amounts of OAS1 were added from 0-2 μM and shifted complexes detected on 5% non-denaturing gels.

Chapter 4

Discussion and Conclusions

4.1 Discussion

VA_I RNA is transcribed in the late stages of infection at high concentration (~μM range) and has been demonstrated to attenuate the activity of a number of key players in the innate immune response including PKR (through competitive inhibition) and the RNA silencing machinery (through processing and incorporating the terminal stem of VA_I into the silencing machinery via the activity of Dicer) (84, 128). Interestingly, a previous report has demonstrated that, *in vitro*, VA_I has the opposite effect on OAS1, an interferon-induced member of the innate immune response (42). We hypothesized that this seemingly contradictory observation could be resolved by investigating VA_I RNA lacking the terminal stem as this would be generated by the RNA silencing machinery. We initiated investigations into a specific OAS1 isoform and examined binding affinity, complex stoichiometry, activation potential, and role of RNA 5'-end modifications in the process. Overall, we can conclude that while full length VA_I is an activator of OAS1 *in vitro*, $VA_I\Delta TS$ is a poor activator (or pseudo-inhibitor), consistent with its role in inhibiting PKR (128). Therefore, Dicer-processed VA_I could potentially serve to downregulate both RNAi and dsRNA responses to viral RNA.

In order to investigate the ability of VA_I RNA to regulate OAS1 activity, it was necessary to develop an efficient OAS1 expression and purification system. In this thesis,

an *E. coli* protein expression system has been developed and optimized for the specific OAS1 p42 isoform. Since OAS1 p42 is the smallest and simplest of human OAS enzymes, we decided to start with this specific isoform. In order to overcome traditional yield and solubility issues, a fusion protein including highly soluble bacterial protein domains, GB1 and NusA, were added to OAS1 (**Fig.6**). The presence of a TEV protease site enables the removal of the fusion tag to generate a monomeric OAS protein confirmed by denaturing SDS-PAGE, non-denaturing MS, and SEC (**Figs.12a, 15a and 9**). Catalytic activity of purified OAS1 was examined by incubating in the presence and absence of a potent synthetic dsRNA activator (poly I:C). The results are consistent with an active enzyme (**Fig.12b**). Due to the additional required step to cleave the GNSHT tag from target protein, the final yield of OAS1 enzyme is 1.5 to 2.0 mg (0.036 to 0.048 μmol) per 1L cell culture, which is sufficient for most biochemical analysis. For protein structural analysis, especially nuclear magnetic resonance (NMR) and x-ray crystallography, the volume of cell culture needs to be scaled up. In term of cost, conventional medium (LB medium) is used and TEV protease is prepared in-house, which makes the cost of this purification procedure significantly lower than the established insect cell system. With regard to time, it takes four days to produce the pure OAS1 protein, including expression, induction and purification procedures. Furthermore, this system can be directly applied to the purification of OAS1 mutants. Establishing OAS expression/purification system represented the majority of the work of this project, but will now be useful for the purification of mutants of different OAS isoforms.

We produced four distinct VA_I RNA molecules to study their potential for activation/inhibition of OAS1. Each RNA was *in vitro* transcribed and purified

extensively following an established purification procedure. Pure RNA species can now be generated in one week at a high yield for biochemical and structural studies. While full-length VA_I served as an activator of OAS1, a terminal stem deleted version of the RNA ($VA_I\Delta TS$) serves as a poor activator of OAS1 relative to other RNAs examined (**Figs.17b and c**). In fact, competition studies with a potent OAS1 activator indicate pseudo-inhibitor behaviour of $VA_I\Delta TS$ (**Fig.17d**). We do not believe that contaminants from *in* vitro transcription or degradation products could be responsible for this behaviour as RNAs are purified by size exclusion chromatography and their homogeneity confirmed by gel electrophoresis. Furthermore, a known ssRNA molecule produced in an identical manner neither activates nor inhibits OAS1 activity. These results are consistent with those observed for PKR, wherein $VA_I\Delta TS$ is an effective PKR inhibitor (128). Removal of the central stem from $VA_I\Delta TS$ results in the formation of a potent OAS1 activator, indicating the central stem prevents OAS1 activation. The role of the central stem still needs to be parsed out, but a plausible hypothesis is that, in a manner similar to that observed for PKR, the central stem sterically precludes OAS1 self-association (40, 81). These results are consistent with a study that has shown that the apical and terminal stems are the key contributors to the activation of OAS1 by full length VA_I RNA (42).

A colorimetric method was developed and employed to examine the OAS1 catalytic activity by detecting PPi generated from the OAS1 enzyme reaction. The amount of PPi indicates the formation of 2'-5'-A chain which reflects the OAS1 reaction rates. This assay does not involve any additional enzymatic reaction or any radioactive reagent, and is sensitive up to 20 nmoles in a 1 ml reaction volume. Another advantage

of this assay is the timesaving feature, as it takes only 2 to 3 hours to finish the whole experiment. When using the potent synthetic dsRNA activator (poly I:C), the detected OAS1 activation level is comparable with other published results (42, 44). Since the formation of 2'-5'-A chain is not measured directly, another method (e.g., radioactive assay) is recommended to validate this assay. We have attempted to employ HPLC (C_{18} reverse phase column) to directly identify 2'-5'-A molecules. Preliminary results (data not shown) demonstrated that after OAS1 reaction the amount of substrate ATP decreased significantly compared with OAS1-free control. We could not identify the 2'-5'-A peak from HPLC spectra since we do not currently have 2'-5'-A standards in hand. Comparison to the radioactive assay, HPLC detection of 2'-5'-A chain formation is another logical step.

The literature presents conflicting reports about the oligomerization state of OAS1 upon activation by dsRNA. While some reports claim that OAS1 tetramerization is required (56, 129), crosslinking experiments have indicated that both the latent and activated form of the enzyme are monomeric (58). While our data do not resolve this conflict, we do not observe tetramer under any conditions examined with VA_I RNA. We focused our attention on the OAS1-$VA_I\Delta$TS interaction, as stable complexes could be analyzed. $VA_I\Delta$TS, forms two distinct complexes as detected by EMSA, and characterization of these complexes by non-denaturing MS identifies these complexes as 1:1 and 2:1 OAS1:$VA_I\Delta$TS (**Fig.15c**). To our knowledge, this is the first non-covalent RNA:protein interaction characterized using this methodology. This method has, however, been used successfully in the characterization of DNA-protein complexes (130, 131). DLS results, which are performed at significantly higher concentrations than

EMSA, indicate that the formation of a monodisperse complex that most likely represents the 2:1 OAS1:RNA complex alone. These results may suggest two independent OAS1 binding sites on the dsRNA molecule, although our data cannot exclude the possibility that OAS1 self-association upon RNA binding is responsible for the interaction.

In our initial protein preparations, OAS1 was purified in the presence of BME (instead of DTT) as a reducing agent, which we later determined by MS covalently modified the OAS1 protein. Interestingly, in this case a single shifted complex was observed by EMSA (**Fig.16a**) and it corresponded to the 1:1 complex of OAS1:$VA_I\Delta TS$ (**Fig.15d**). When DTT was used instead of BME, two shifted complexes were observed by EMSA (**Fig.16b**) and it corresponded to the 1:1 and 2:1 complexes of OAS1:$VA_I\Delta TS$ (**Fig.15c**). Therefore, it appears likely that the covalent modification of OAS1 with BME serves to disrupt an important interaction, and we recommend abandoning its use in the examination of OAS1 enzymes.

A previous study of the activation of oligoadenlyate synthetases by double-stranded RNA aptamers demonstrated that a given RNA activator could be fit to a kinetic model where the apparent dissociation constant (K_{app}) and the maximal reaction velocity (V_{max}) were demonstrated to behave as independent variables (60). The VA_I RNA molecules used in this study showed similar behaviour when fit to the kinetic model (**Table 1**). Comparison of VA_I to $VA_I\Delta TS$, the most biologically relevant example, reveals that while $VA_I\Delta TS$ has a significantly reduced V_{max}, it has a greater affinity for OAS1 than the full-length VA_I. This would be beneficial in terms of inhibition as the processed version of VA_I could outcompete RNA activators with lower affinities.

Therefore flooding host cell with VA_I RNA represents an effective mechanism to suppress the OAS1-mediated innate immune response. These results reinforce the importance of understanding both the binding affinity and activation potential for potential binding partners of OAS enzymes, as consideration of each parameter independently can lead to misinterpretation.

The mechanism of OAS1 activation is thought to proceed through a two-step process (60). First, dsRNA binds to the OAS enzyme in a relatively non-specific way followed by a conformation change to OAS enzyme structure. However the fate of the RNA throughout the activation process remains a key piece of information not fully understood. When incubated for 90 minutes sufficient for OAS1 activation, dissociation of the OAS1-$VA_I\Delta TS$ complex is observed under activating conditions (both ATP and Mg^{2+} present) (**Fig.18a**). This observation indicates that dsRNA does not remain associated with OAS1 under conditions that lead to catalytic competence. This hypothesis is supported by previous observations for PKR, wherein the dsRNA release was observed after autophosphorylation of PKR (132).

One of the suggested mechanisms whereby the innate immune system differentiates foreign from host dsRNA is via the modification of 5'-end phosphorylation state (89). VA_I RNA is transcribed as an unmodified, non-polyadenylated transcript that accumulates in the cytoplasm at late times of infection (74). We have highlighted the importance of the nature of the 5'-end of VA_I RNA to the catalytic activation of the enzyme. $VA_I\Delta TS$ wherein the 5'-end possessed either (i) the *in vitro* modification, a 5'-triphosphate (5'-PPP), (ii) the typical *in vivo* modification after processing a monophosphate (5'-P), or (iii) a 5'-end devoid of phosphates (5'-OH) revealed that the

5’-P and 5’-OH demonstrated a significantly reduced ability to stimulate 2’-5’-A formation via OAS1 (**Fig.19a**). Affinity of $VA_I\Delta TS$ RNA for OAS1 is similar whether a 5’-PPP or 5’-P is present, however the RNA construct lacking 5’-phosphates (5’-OH) had a significantly reduced affinity for OAS1 (**Fig.19b**). These data suggest an inhibitory mechanism whereby Dicer cleavage of VA_I to $VA_I\Delta TS$ generates an RNA molecule that maximizes its ability to interact with and suppress OAS1 activity. Preliminary examination of VA_I-AS indicates that the phosphorylation state present at the 5’-end of RNA may represent a more general phenomenon in the activation of OAS1, and will require an extensive examination of a variety of dsRNA molecules to confirm. However, these initial results are supported by the observation that the presence of an intact 5’-triphosphate is necessary for the innate immune responses mediated by other dsRNA responders, including RIG-I and PKR (89).

4.2 Conclusions

This thesis set out to characterize the particular regions of VA_I RNA that contribute to the activation of OAS, to determine the regulatory effect of VA_I RNA on OAS activity, and to identify the structural characteristics of OAS-VA_I RNA complex. Using a combination of biochemical approaches, both VA_I RNA-protein complex formation and OAS1 activation/inhibition potential of these RNA molecules have been characterized. Additionally, the importance of RNA 5’-end phosphorylation state to its regulatory ability for OAS1 activity has been investigated. This study confirms previous findings that VA_I RNA can activate OAS1 enzyme and contributes additional evidence

that suggests that physiologically important Dicer-processed VA_I lacking the terminal stem acts as a pseudo-inhibitor of OAS1.

Figure 20 VA_I simultaneously antagonize both the RNAi machinery and the IFN-inducible antiviral proteins

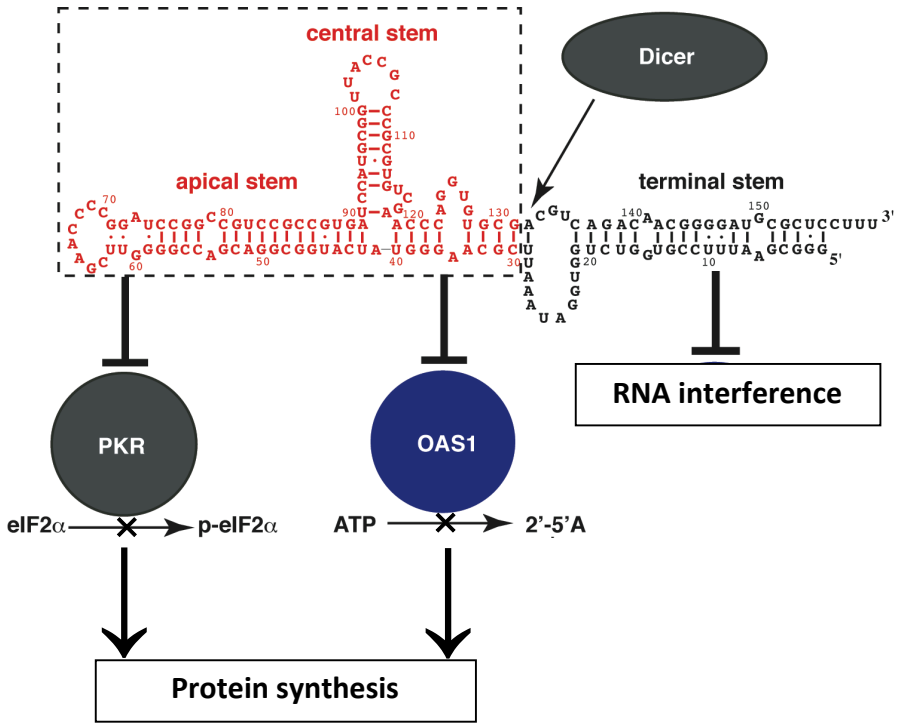

The Dicer-processed version of VA_I RNA lacking terminal stem inhibits the activation of both PKR and OAS enzymes to enable protein synthesis required for virus replication. Also, the terminal stem is incorporated into the RNAi machinery to suppress RNA interference.

The findings from this thesis suggest a model (**Fig.20**) illustrating interaction mechanism between VA_I RNA and its protein partners of the innate immune response. The Dicer-processed version of VA_I RNA lacking terminal stem inhibits the activation of

both PKR and OAS enzymes, two key IFN-inducible antiviral proteins, to enable the protein synthesis required for virus replication in virus-infected cells. VA_I RNA also binds Dicer via its terminal stem to competitively block Dicer enzyme to eventually suppress RNAi responses to viral infection. Taken together, the current data suggests a plausible strategy whereby adenoviruses use a single VA_I RNA transcript to simultaneously antagonize both the RNAi machinery (via a processed terminal stem) and the interferon response (via the remaining apical and central stems).

4.3 Future studies

Since the current thesis only focuses on the regulation of OAS1 enzymes, it is recommended that further investigations be undertaken by using the experimental approaches of this thesis in the following areas:

(i) Further examination of different OAS variants, particularly OAS2/OAS3 isoforms is required to understand the molecular basis for their regulation by viral dsRNAs. The *E. coli* expression and purification procedure established in this thesis can be used for structural studies of other OAS variants, particularly OAS2/OAS3. However, it is critical to express these proteins in human cells for cellular and functional investigations because post-translational modifications are thought to be required for these isoforms. I made attempts to express OAS1 enzyme in HEK293T cell, but results from the trial experiments were not successful at the molecular cloning stage (data not shown).

(ii) This thesis was unsuccessful at resolving the conflict about the oligomerization state of OAS1 upon binding by dsRNA. By EMSA and non-denaturing

MS, 2:1 OAS1:$VA_I\Delta TS$ have been observed, however, no OAS1:$VA_I\Delta TS$ complex has been purified by size exclusion chromatography. Crosslinking of OAS1 with its RNA cofactors by UV radiation or chemical coupling agents could be a solution to solve these problems. Since $VA_I\Delta TS$ behaves as a pseudo-inhibitor for OAS1 *in vitro*, it cannot be ruled out that $VA_I\Delta TS$ prevents OAS1 enzyme from forming tetramer. Thus, it is necessary to investigate OAS1 oligomerization state upon binding by a potent RNA activator by employing the same experimental methodologies as used for $VA_I\Delta TS$.

(iii) Further investigation using the same experimental set-up is recommended for other viral dsRNA, particularly $EBER_I$ RNA, since it has similar secondary structure and inhibitory effects on PKR as VA_I RNA. It would be interesting to determine the regulatory effect of $EBER_I$ RNA version lacking the TS stem on both PKR and OAS enzymes for comparison.

(iv) Preliminary examination of the 5'-end phosphorylation state of RNA indicates that 5'-end modification is important to the catalytic activation of OAS1 enzymes. We compared the OAS1 binding affinity and activation potential of VA_I RNA with three different 5'-ends (5'-PPP, 5'-P, and 5'-OH). Further investigation is recommended to examine the effect of 7-methylguanosine capped RNA on OAS1 activation. Also, a detailed kinetic analysis should be performed on 5'-end modified RNAs.

(v) The current thesis was unable to initiate high-resolution structural studies (particularly, NMR and x-ray crystallography) for OAS1-dsRNA complexes. Future

studies should therefore concentrate on resolving high-resolution structures of OAS enzymes and OAS-dsRNA complexes.

References

1. Li XL, Ezelle HJ, Hsi TY, Hassel BA. A central role for RNA in the induction and biological activities of type 1 interferons. Wiley Interdiscip Rev RNA. 2011 Jan-Feb;2(1):58-78.

2. David M. Interferons and microRNAs. J Interferon Cytokine Res. 2010 Nov;30(11):825-8.

3. Randall RE, Goodbourn S. Interferons and viruses: An interplay between induction, signalling, antiviral responses and virus countermeasures. J Gen Virol. 2008 Jan;89(Pt 1):1-47.

4. Weber F, Kochs G, Haller O. Inverse interference: How viruses fight the interferon system. Viral Immunol. 2004;17(4):498-515.

5. Sen GC, Sarkar SN. The interferon-stimulated genes: Targets of direct signaling by interferons, double-stranded RNA, and viruses. Curr Top Microbiol Immunol. 2007;316:233-50.

6. Karpala AJ, Doran TJ, Bean AG. Immune responses to dsRNA: Implications for gene silencing technologies. Immunol Cell Biol. 2005 Jun;83(3):211-6.

7. Malmgaard L. Induction and regulation of IFNs during viral infections. J Interferon Cytokine Res. 2004 Aug;24(8):439-54.

8. Sadler AJ, Williams BR. Interferon-inducible antiviral effectors. Nat Rev Immunol. 2008 Jul;8(7):559-68.

9. Sioud M. Innate sensing of self and non-self RNAs by toll-like receptors. Trends Mol Med. 2006 Apr;12(4):167-76.

10. Matsumoto M, Seya T. TLR3: Interferon induction by double-stranded RNA including poly(I:C). Adv Drug Deliv Rev. 2008 Apr 29;60(7):805-12.

11. Jiang Z, Mak TW, Sen G, Li X. Toll-like receptor 3-mediated activation of NF-kappaB and IRF3 diverges at toll-IL-1 receptor domain-containing adapter inducing IFN-beta. Proc Natl Acad Sci U S A. 2004 Mar 9;101(10):3533-8.

12. Kato H, Takahasi K, Fujita T. RIG-I-like receptors: Cytoplasmic sensors for non-self RNA. Immunol Rev. 2011 Sep;243(1):91-8.

13. Matsumoto M, Funami K, Tanabe M, Oshiumi H, Shingai M, Seto Y, et al. Subcellular localization of toll-like receptor 3 in human dendritic cells. J Immunol. 2003 Sep 15;171(6):3154-62.

14. Wang Y, Liu L, Davies DR, Segal DM. Dimerization of toll-like receptor 3 (TLR3) is required for ligand binding. J Biol Chem. 2010 Nov 19;285(47):36836-41.

15. Meylan E, Burns K, Hofmann K, Blancheteau V, Martinon F, Kelliher M, et al. RIP1 is an essential mediator of toll-like receptor 3-induced NF-kappa B activation. Nat Immunol. 2004 May;5(5):503-7.

16. Caamano J, Hunter CA. NF-kappaB family of transcription factors: Central regulators of innate and adaptive immune functions. Clin Microbiol Rev. 2002 Jul;15(3):414-29.

17. Loo YM, Fornek J, Crochet N, Bajwa G, Perwitasari O, Martinez-Sobrido L, et al. Distinct RIG-I and MDA5 signaling by RNA viruses in innate immunity. J Virol. 2008 Jan;82(1):335-45.

18. Satoh T, Kato H, Kumagai Y, Yoneyama M, Sato S, Matsushita K, et al. LGP2 is a positive regulator of RIG-I- and MDA5-mediated antiviral responses. Proc Natl Acad Sci U S A. 2010 Jan 26;107(4):1512-7.

19. Takaoka A, Yanai H. Interferon signalling network in innate defence. Cell Microbiol. 2006 Jun;8(6):907-22.

20. Kumaran J, Wei L, Kotra LP, Fish EN. A structural basis for interferon-alpha-receptor interactions. FASEB J. 2007 Oct;21(12):3288-96.

21. Kim SH, Cohen B, Novick D, Rubinstein M. Mammalian type I interferon receptors consists of two subunits: IFNaR1 and IFNaR2. Gene. 1997 Sep 1;196(1-2):279-86.

22. Bluyssen AR, Durbin JE, Levy DE. ISGF3 gamma p48, a specificity switch for interferon activated transcription factors. Cytokine Growth Factor Rev. 1996 Jun;7(1):11-7.

23. Li X, Leung S, Qureshi S, Darnell JE,Jr, Stark GR. Formation of STAT1-STAT2 heterodimers and their role in the activation of IRF-1 gene transcription by interferon-alpha. J Biol Chem. 1996 Mar 8;271(10):5790-4.

24. Sarkar SN, Sen GC. Novel functions of proteins encoded by viral stress-inducible genes. Pharmacol Ther. 2004 Sep;103(3):245-59.

25. Hovanessian AG. On the discovery of interferon-inducible, double-stranded RNA activated enzymes: The 2'-5'oligoadenylate synthetases and the protein kinase PKR. Cytokine Growth Factor Rev. 2007 Oct-Dec;18(5-6):351-61.

26. Malathi K, Dong B, Gale M,Jr, Silverman RH. Small self-RNA generated by RNase L amplifies antiviral innate immunity. Nature. 2007 Aug 16;448(7155):816-9.

27. Williams BR. Signal integration via PKR. Sci STKE. 2001 Jul 3;2001(89):re2.

28. Sarkar SN, Miyagi M, Crabb JW, Sen GC. Identification of the substrate-binding sites of 2'-5'-oligoadenylate synthetase. J Biol Chem. 2002 Jul 5;277(27):24321-30.

29. Sarkar SN, Ghosh A, Wang HW, Sung SS, Sen GC. The nature of the catalytic domain of 2'-5'-oligoadenylate synthetases. J Biol Chem. 1999 Sep 3;274(36):25535-42.

30. Silverman RH. Viral encounters with 2',5'-oligoadenylate synthetase and RNase L during the interferon antiviral response. J Virol. 2007 Dec;81(23):12720-9.

31. Wreschner DH, James TC, Silverman RH, Kerr IM. Ribosomal RNA cleavage, nuclease activation and 2-5A(ppp(A2'p)nA) in interferon-treated cells. Nucleic Acids Res. 1981 Apr 10;9(7):1571-81.

32. Malathi K, Saito T, Crochet N, Barton DJ, Gale M,Jr, Silverman RH. RNase L releases a small RNA from HCV RNA that refolds into a potent PAMP. RNA. 2010 Nov;16(11):2108-19.

33. Malathi K, Dong B, Gale M,Jr, Silverman RH. Small self-RNA generated by RNase L amplifies antiviral innate immunity. Nature. 2007 Aug 16;448(7155):816-9.

34. McKenna SA, Lindhout DA, Shimoike T, Puglisi JD. Biophysical and biochemical investigations of dsRNA-activated kinase PKR. Methods Enzymol. 2007;430:373-96.

35. Pindel A, Sadler A. The role of protein kinase R in the interferon response. J Interferon Cytokine Res. 2011 Jan;31(1):59-70.

36. Farrell PJ, Sen GC, Dubois MF, Ratner L, Slattery E, Lengyel P. Interferon action: Two distinct pathways for inhibition of protein synthesis by double-stranded RNA. Proc Natl Acad Sci U S A. 1978 Dec;75(12):5893-7.

37. Sadler AJ, Latchoumanin O, Hawkes D, Mak J, Williams BR. An antiviral response directed by PKR phosphorylation of the RNA helicase A. PLoS Pathog. 2009 Feb;5(2):e1000311.

38. Endo-Munoz L, Warby T, Harrich D, McMillan NA. Phosphorylation of HIV tat by PKR increases interaction with TAR RNA and enhances transcription. Virol J. 2005 Feb 28;2:17.

39. Bonnet MC, Weil R, Dam E, Hovanessian AG, Meurs EF. PKR stimulates NF-kappaB irrespective of its kinase function by interacting with the IkappaB kinase complex. Mol Cell Biol. 2000 Jul;20(13):4532-42.

40. McKenna SA, Lindhout DA, Shimoike T, Aitken CE, Puglisi JD. Viral dsRNA inhibitors prevent self-association and autophosphorylation of PKR. J Mol Biol. 2007 Sep 7;372(1):103-13.

41. Sharp TV, Raine DA, Gewert DR, Joshi B, Jagus R, Clemens MJ. Activation of the interferon-inducible (2'-5') oligoadenylate synthetase by the epstein-barr virus RNA, EBER-1. Virology. 1999 May 10;257(2):303-13.

42. Desai SY, Patel RC, Sen GC, Malhotra P, Ghadge GD, Thimmapaya B. Activation of interferon-inducible 2’-5’oligoadenylate synthetase by adenoviral VAI RNA. J Biol Chem. 1995 Feb 17;270(7):3454-61.

43. Mordechai E, Kon N, Henderson EE, Suhadolnik RJ. Activation of the interferon-inducible enzymes, 2',5'-oligoadenylate synthetase and PKR by human T-cell leukemia virus type I rex-response element. Virology. 1995 Feb 1;206(2):913-22.

44. Maitra RK, McMillan NA, Desai S, McSwiggen J, Hovanessian AG, Sen G, et al. HIV-1 TAR RNA has an intrinsic ability to activate interferon-inducible enzymes. Virology. 1994 Nov 1;204(2):823-7.

45. Townsend HL, Jha BK, Han JQ, Maluf NK, Silverman RH, Barton DJ. A viral RNA competitively inhibits the antiviral endoribonuclease domain of RNase L. RNA. 2008 Jun;14(6):1026-36.

46. Han JQ, Townsend HL, Jha BK, Paranjape JM, Silverman RH, Barton DJ. A phylogenetically conserved RNA structure in the poliovirus open reading frame inhibits the antiviral endoribonuclease RNase L. J Virol. 2007 Jun;81(11):5561-72.

47. Zilberstein A, Kimchi A, Schmidt A, Revel M. Isolation of two interferon-induced translational inhibitors: A protein kinase and an oligo-isoadenylate synthetase. Proc Natl Acad Sci U S A. 1978 Oct;75(10):4734-8.

48. Kerr IM, Williams BR, Hovanessian AG, Brown RE, Martin EM, Gilbert CS, et al. Cell-free protein synthesis and interferon action: Protein kinase(s) and an oligonucleotide effector, pppA2'p5'A2'p5'A. Haematol Blood Transfus. 1979;23:291-4.

49. Chakrabarti A, Jha BK, Silverman RH. New insights into the role of RNase L in innate immunity. J Interferon Cytokine Res. 2011 Jan;31(1):49-57.

50. Hovanessian AG, Justesen J. The human 2'-5'oligoadenylate synthetase family: Unique interferon-inducible enzymes catalyzing 2’-5’instead of 3'-5' phosphodiester bond formation. Biochimie. 2007 Jun-Jul;89(6-7):779-88.

51. Hovnanian A, Rebouillat D, Mattei MG, Levy ER, Marie I, Monaco AP, et al. The human 2',5'-oligoadenylate synthetase locus is composed of three distinct genes clustered on chromosome 12q24.2 encoding the 100-, 69-, and 40-kDa forms. Genomics. 1998 Sep 15;52(3):267-77.

52. Bonnevie-Nielsen V, Field LL, Lu S, Zheng DJ, Li M, Martensen PM, et al. Variation in antiviral 2',5'-oligoadenylate synthetase (2'5'AS) enzyme activity is controlled by a single-nucleotide polymorphism at a splice-acceptor site in the OAS1 gene. Am J Hum Genet. 2005 Apr;76(4):623-33.

53. Hartmann R, Olsen HS, Widder S, Jorgensen R, Justesen J. p59OASL, a 2’-5’oligoadenylate synthetase like protein: A novel human gene related to the 2’-5’oligoadenylate synthetase family. Nucleic Acids Res. 1998 Sep 15;26(18):4121-8.

54. Marques J, Anwar J, Eskildsen-Larsen S, Rebouillat D, Paludan SR, Sen G, et al. The p59 oligoadenylate synthetase-like protein possesses antiviral activity that requires the C-terminal ubiquitin-like domain. J Gen Virol. 2008 Nov;89(Pt 11):2767-72.

55. Marie I, Svab J, Robert N, Galabru J, Hovanessian AG. Differential expression and distinct structure of 69- and 100-kDa forms of 2-5A synthetase in human cells treated with interferon. J Biol Chem. 1990 Oct 25;265(30):18601-7.

56. Ghosh A, Sarkar SN, Guo W, Bandyopadhyay S, Sen GC. Enzymatic activity of 2'-5'-oligoadenylate synthetase is impaired by specific mutations that affect oligomerization of the protein. J Biol Chem. 1997 Dec 26;272(52):33220-6.

57. Wathelet M, Moutschen S, Cravador A, DeWit L, Defilippi P, Huez G, et al. Full-length sequence and expression of the 42 kDa 2-5A synthetase induced by human interferon. FEBS Lett. 1986 Feb 3;196(1):113-20.

58. Hartmann R, Walko G, Justesen J. Inhibition of 2’-5’oligoadenylate synthetase by divalent metal ions. FEBS Lett. 2001 Oct 19;507(1):54-8.

59. Hartmann R, Justesen J, Sarkar SN, Sen GC, Yee VC. Crystal structure of the 2'-specific and double-stranded RNA-activated interferon-induced antiviral protein 2'-5'-oligoadenylate synthetase. Mol Cell. 2003 Nov;12(5):1173-85.

60. Hartmann R, Norby PL, Martensen PM, Jorgensen P, James MC, Jacobsen C, et al. Activation of 2’-5’oligoadenylate synthetase by single-stranded and double-stranded RNA aptamers. J Biol Chem. 1998 Feb 6;273(6):3236-46.

61. Desai SY, Sen GC. Effects of varying lengths of double-stranded RNA on binding and activation of 2'-5'-oligoadenylate synthetase. J Interferon Cytokine Res. 1997 Sep;17(9):531-6.

62. Kodym R, Kodym E, Story MD. 2'-5'-oligoadenylate synthetase is activated by a specific RNA sequence motif. Biochem Biophys Res Commun. 2009 Oct 16;388(2):317-22.

63. Baglioni C, Minks MA, De Clercq E. Structural requirements of polynucleotides for the activation of (2' - 5')an polymerase and protein kinase. Nucleic Acids Res. 1981 Oct 10;9(19):4939-50.

64. Anderson BR, Muramatsu H, Jha BK, Silverman RH, Weissman D, Kariko K. Nucleoside modifications in RNA limit activation of 2'-5'-oligoadenylate synthetase and increase resistance to cleavage by RNase L. Nucleic Acids Res. 2011 Nov;39(21):9329-38.

65. Torralba S, Sojat J, Hartmann R. 2’-5’oligoadenylate synthetase shares active site architecture with the archaeal CCA-adding enzyme. Cell Mol Life Sci. 2008 Aug;65(16):2613-20.

66. Marie I, Blanco J, Rebouillat D, Hovanessian AG. 69-kDa and 100-kDa isoforms of interferon-induced (2'-5')oligoadenylate synthetase exhibit differential catalytic parameters. Eur J Biochem. 1997 Sep 1;248(2):558-66.

67. Rebouillat D, Hovnanian A, Marie I, Hovanessian AG. The 100-kDa 2',5'-oligoadenylate synthetase catalyzing preferentially the synthesis of dimeric pppA2'p5'A

molecules is composed of three homologous domains. J Biol Chem. 1999 Jan 15;274(3):1557-65.

68. Liang SL, Quirk D, Zhou A. RNase L: Its biological roles and regulation. IUBMB Life. 2006 Sep;58(9):508-14.

69. Tanaka N, Nakanishi M, Kusakabe Y, Goto Y, Kitade Y, Nakamura KT. Structural basis for recognition of 2',5'-linked oligoadenylates by human ribonuclease L. EMBO J. 2004 Oct 13;23(20):3929-38.

70. Tanaka N, Nakanishi M, Kusakabe Y, Goto Y, Kitade Y, Nakamura KT. Molecular basis for recognition of 2',5'-linked oligoadenylates by the N-terminal ankyrin repeat domain of human ribonuclease L. Nucleic Acids Symp Ser (Oxf). 2005;(49) (49):323-4.

71. Castelli JC, Hassel BA, Maran A, Paranjape J, Hewitt JA, Li XL, et al. The role of 2'-5'oligoadenylate-activated ribonuclease L in apoptosis. Cell Death Differ. 1998 Apr;5(4):313-20.

72. Lynch JP,3rd, Fishbein M, Echavarria M. Adenovirus. Semin Respir Crit Care Med. 2011 Aug;32(4):494-511.

73. Ma Y, Mathews MB. Structure, function, and evolution of adenovirus-associated RNA: A phylogenetic approach. J Virol. 1996 Aug;70(8):5083-99.

74. Ma Y, Mathews MB. Comparative analysis of the structure and function of adenovirus virus-associated RNAs. J Virol. 1993 Nov;67(11):6605-17.

75. Mathews MB. Structure, function, and evolution of adenovirus virus-associated RNAs. Curr Top Microbiol Immunol. 1995;199 (Pt 2) (Pt 2):173-87.

76. Coventry VK, Conn GL. Analysis of adenovirus VA RNAI structure and stability using compensatory base pair modifications. Nucleic Acids Res. 2008 Mar;36(5):1645-53.

77. Minamitani T, Iwakiri D, Takada K. Adenovirus virus-associated RNAs induce type I interferon expression through a RIG-I-mediated pathway. J Virol. 2011 Apr;85(8):4035-40.

78. Aparicio O, Razquin N, Zaratiegui M, Narvaiza I, Fortes P. Adenovirus virus-associated RNA is processed to functional interfering RNAs involved in virus production. J Virol. 2006 Feb;80(3):1376-84.

79. Ghadge GD, Malhotra P, Furtado MR, Dhar R, Thimmapaya B. In vitro analysis of virus-associated RNA I (VAI RNA): Inhibition of the double-stranded RNA-activated protein kinase PKR by VAI RNA mutants correlates with the in vivo phenotype and the structural integrity of the central domain. J Virol. 1994 Jul;68(7):4137-51.

80. Lei M, Liu Y, Samuel CE. Adenovirus VAI RNA antagonizes the RNA-editing activity of the ADAR adenosine deaminase. Virology. 1998 Jun 5;245(2):188-96.

81. McKenna SA, Kim I, Liu CW, Puglisi JD. Uncoupling of RNA binding and PKR kinase activation by viral inhibitor RNAs. J Mol Biol. 2006 May 19;358(5):1270-85.

82. Cheng JC, Moore TB, Sakamoto KM. RNA interference and human disease. Mol Genet Metab. 2003 Sep-Oct;80(1-2):121-8.

83. Bernstein E, Caudy AA, Hammond SM, Hannon GJ. Role for a bidentate ribonuclease in the initiation step of RNA interference. Nature. 2001 Jan 18;409(6818):363-6.

84. Andersson MG, Haasnoot PC, Xu N, Berenjian S, Berkhout B, Akusjarvi G. Suppression of RNA interference by adenovirus virus-associated RNA. J Virol. 2005 Aug;79(15):9556-65.

85. Wahid AM, Coventry VK, Conn GL. The PKR-binding domain of adenovirus VA RNAI exists as a mixture of two functionally non-equivalent structures. Nucleic Acids Res. 2009 Sep;37(17):5830-7.

86. Sano M, Kato Y, Taira K. Sequence-specific interference by small RNAs derived from adenovirus VAI RNA. FEBS Lett. 2006 Mar 6;580(6):1553-64.

87. Hornung V, Ellegast J, Kim S, Brzozka K, Jung A, Kato H, et al. 5'-triphosphate RNA is the ligand for RIG-I. Science. 2006 Nov 10;314(5801):994-7.

88. Marques JT, Devosse T, Wang D, Zamanian-Daryoush M, Serbinowski P, Hartmann R, et al. A structural basis for discriminating between self and nonself double-stranded RNAs in mammalian cells. Nat Biotechnol. 2006 May;24(5):559-65.

89. Nallagatla SR, Toroney R, Bevilacqua PC. A brilliant disguise for self RNA: 5'-end and internal modifications of primary transcripts suppress elements of innate immunity. RNA Biol. 2008 Jul-Sep;5(3):140-4.

90. Hocine S, Singer RH, Grunwald D. RNA processing and export. Cold Spring Harb Perspect Biol. 2010 Dec;2(12):a000752.

91. Nallagatla SR, Hwang J, Toroney R, Zheng X, Cameron CE, Bevilacqua PC. 5'-triphosphate-dependent activation of PKR by RNAs with short stem-loops. Science. 2007 Nov 30;318(5855):1455-8.

92. Sharp TV, Schwemmle M, Jeffrey I, Laing K, Mellor H, Proud CG, et al. Comparative analysis of the regulation of the interferon-inducible protein kinase PKR by epstein-barr virus RNAs EBER-1 and EBER-2 and adenovirus VAI RNA. Nucleic Acids Res. 1993 Sep 25;21(19):4483-90.

93. McCormack SJ, Samuel CE. Mechanism of interferon action: RNA-binding activity of full-length and R-domain forms of the RNA-dependent protein kinase PKR--determination of KD values for VAI and TAR RNAs. Virology. 1995 Jan 10;206(1):511-9.

94. Lin RJ, Yu HP, Chang BL, Tang WC, Liao CL, Lin YL. Distinct antiviral roles for human 2',5'-oligoadenylate synthetase family members against dengue virus infection. J Immunol. 2009 Dec 15;183(12):8035-43.

95. Ball LA. Induction, purification, and properties of 2'5' oligoadenylate synthetase. Ann N Y Acad Sci. 1980;350:486-96.

96. Wells JA, Swyryd EA, Stark GR. An improved method for purifying 2',5'-oligoadenylate synthetases. J Biol Chem. 1984 Jan 25;259(2):1363-70.

97. Mory Y, Vaks B, Chebath J. Production of two human 2',5'-oligoadenylate synthetase enzymes in escherichia coli. J Interferon Res. 1989 Jun;9(3):295-304.

98. Bandyopadhyay S, Ghosh A, Sarkar SN, Sen GC. Production and purification of recombinant 2'-5'oligoadenylate synthetase and its mutants using the baculovirus system. Biochemistry. 1998 Mar 17;37(11):3824-30.

99. Kon N, Suhadolnik RJ. Identification of the ATP binding domain of recombinant human 40-kDa 2',5'-oligoadenylate synthetase by photoaffinity labeling with 8-azido-[alpha-32P]ATP. J Biol Chem. 1996 Aug 16;271(33):19983-90.

100. Sarkar SN, Sen GC. Production, purification, and characterization of recombinant 2', 5'-oligoadenylate synthetases. Methods. 1998 Jul;15(3):233-42.

101. Ghosh A, Desai SY, Sarkar SN, Ramaraj P, Ghosh SK, Bandyopadhyay S, et al. Effects of mutating specific residues present near the amino terminus of 2'-5'-oligoadenylate synthetase. J Biol Chem. 1997 Jun 13;272(24):15452-8.

102. Agilent Thchnologies. BL21-CodonPlus competent cells instruction manual.

103. Hammarstrom M, Hellgren N, van Den Berg S, Berglund H, Hard T. Rapid screening for improved solubility of small human proteins produced as fusion proteins in escherichia coli. Protein Sci. 2002 Feb;11(2):313-21.

104. Waugh DS. Making the most of affinity tags. Trends Biotechnol. 2005 Jun;23(6):316-20.

105. Waugh DS. An overview of enzymatic reagents for the removal of affinity tags. Protein Expr Purif. 2011 Dec;80(2):283-93.

106. Shevchenko A, Tomas H, Havlis J, Olsen JV, Mann M. In-gel digestion for mass spectrometric characterization of proteins and proteomes. Nat Protoc. 2006;1(6):2856-60.

107. Loboda AV, Krutchinsky AN, Bromirski M, Ens W, Standing KG. A tandem quadrupole/time-of-flight mass spectrometer with a matrix-assisted laser desorption/ionization source: Design and performance. Rapid Commun Mass Spectrom. 2000;14(12):1047-57.

108. Shevchenko A, Loboda A, Shevchenko A, Ens W, Standing KG. MALDI quadrupole time-of-flight mass spectrometry: A powerful tool for proteomic research. Anal Chem. 2000 May 1;72(9):2132-41.

109. Caruthers MH. A brief review of DNA and RNA chemical synthesis. Biochem Soc Trans. 2011 Apr;39(2):575-80.

110. Milligan JF, Groebe DR, Witherell GW, Uhlenbeck OC. Oligoribonucleotide synthesis using T7 RNA polymerase and synthetic DNA templates. Nucleic Acids Res. 1987 Nov 11;15(21):8783-98.

111. Lukavsky PJ, Puglisi JD. Large-scale preparation and purification of polyacrylamide-free RNA oligonucleotides. RNA. 2004 May;10(5):889-93.

112. Cunningham L, Kittikamron K, Lu Y. Preparative-scale purification of RNA using an efficient method which combines gel electrophoresis and column chromatography. Nucleic Acids Res. 1996 Sep 15;24(18):3647-8.

113. Madadlou A, O'Sullivan S, Sheehan D. Fast protein liquid chromatography. Methods Mol Biol. 2011;681:439-47.

114. Booy EP, Meng H, McKenna SA. Nativa RNA purification by gel filtration chromatography. In: Conn GL, editor. Recombinant and *In Vitro* RNA synthesis. New York City, USA: Humana Press; 2012.

115. McKenna SA, Kim I, Puglisi EV, Lindhout DA, Aitken CE, Marshall RA, et al. Purification and characterization of transcribed RNAs using gel filtration chromatography. Nat Protoc. 2007;2(12):3270-7.

116. Sarkar SN, Pandey M, Sen GC. Assays for the interferon-induced enzyme 2',5' oligoadenylate synthetases. Methods Mol Med. 2005;116:81-101.

117. Hassel BA, Ts'o PO. A sensitive assay for the IFN-regulated 2-5A synthetase enzyme. J Virol Methods. 1994 Dec;50(1-3):323-34.

118. Kuusksalu A, Subbi J, Pehk T, Reintamm T, Muller WE, Kelve M. Identification of the reaction products of (2'-5')oligoadenylate synthetase in the marine sponge. Eur J Biochem. 1998 Oct 15;257(2):420-6.

119. Suzuki H, Buonamassa DT. Determination of the level of the core of 2',5'-oligoadenylates by high performance liquid chromatography. Biomed Chromatogr. 1992 Jan-Feb;6(1):35-8.

120. Miele MB, Liu DK, Kan NC. Fractionation and characterization of 2',5'-oligoadenylates by polyacrylamide gel electrophoresis: An alternative method for assaying 2',5'-oligoadenylate synthetase. J Interferon Res. 1991 Feb;11(1):33-40.

121. Tong WB, Zhang CY, Feng BF, Tao QM. Establishment of a nonradioactive assay for 2’-5’oligoadenylate synthetase and its application in chronic hepatitis C patients receiving interferon-alpha. World J Gastroenterol. 1998 Feb;4(1):70-3.

122. Justesen J, Kjeldgaard NO. Spectrophotometric pyrophosphate assay of 2',5'-oligoadenylate synthetase. Anal Biochem. 1992 Nov 15;207(1):90-3.

123. Putnins RF, Yamada EW. Colorimetric determination of inorganic pyrophosphate by a manual or automated method. Anal Biochem. 1975 Sep;68(1):185-95.

124. Justesen J, Kjeldgaard NO. Spectrophotometric pyrophosphate assay of 2',5'-oligoadenylate synthetase. Anal Biochem. 1992 Nov 15;207(1):90-3.

125. Ryder SP, Recht MI, Williamson JR. Quantitative analysis of protein-RNA interactions by gel mobility shift. Methods Mol Biol. 2008;488:99-115.

126. Donald LJ, Dickworth HW, Standing KG. Mass spectrometry in noncovalent protein interactions and protein assemblies. In: Celis J, editor. *Cell Biology: A Laboratory Handbook*. 3rd ed. San Diego, CA: Elsevier Science Inc.; 2006. p. 457-64.

127. Kozlovski VI, Donald LJ, Colado VM, Spicer V, Loboda AV, Chernushevich IV. A TOF mass spectrometer for the study of noncovalent complexes. Int J Mass Spectrum. 2011;308:118-25.

128. Wahid AM, Coventry VK, Conn GL. Systematic deletion of the adenovirus-associated RNAI terminal stem reveals a surprisingly active RNA inhibitor of double-stranded RNA-activated protein kinase. J Biol Chem. 2008 Jun 20;283(25):17485-93.

129. Rebouillat D, Hovanessian AG. The human 2',5'-oligoadenylate synthetase family: Interferon-induced proteins with unique enzymatic properties. J Interferon Cytokine Res. 1999 Apr;19(4):295-308.

130. Potier N, Donald LJ, Chernushevich I, Ayed A, Ens W, Arrowsmith CH, et al. Study of a noncovalent trp repressor: DNA operator complex by electrospray ionization time-of-flight mass spectrometry. Protein Sci. 1998 Jun;7(6):1388-95.

131. Donald LJ, Hosfield DJ, Cuvelier SL, Ens W, Standing KG, Duckworth HW. Mass spectrometric study of the escherichia coli repressor proteins, Ic1R and Gc1R, and their complexes with DNA. Protein Sci. 2001 Jul;10(7):1370-80.

132. McKenna SA, Limdhout DA, Kim I, Liu CW, Gelev VM, Wagner G, Puglisi JD. Molecular framwwork for the activation of RNA-depentent protein kinese. J Biol Chem. 2007 Apr 13;282(15):11474-86.